

A TRANSFORMATIONAL APPROACH TO WINTER OROGRAPHIC WEATHER MODIFICATION RESEARCH

The SNOWIE Project

SARAH A. TESSENDORF, JEFFREY R. FRENCH, KATJA FRIEDRICH, BART GEERTS, ROBERT M. RAUBER,
ROY M. RASMUSSEN, LULIN XUE, KYOKO IKEDA, DEREK R. BLESTRUD, MELVIN L. KUNKEL, SHAUN PARKINSON,
JEFFERSON R. SNIDER, JOSHUA AIKINS, SPENCER FABER, ADAM MAJEWSKI, COLTIN GRASMICK, PHILIP T. BERGMAIER,
ANDREW JANISZESKI, ADAM SPRINGER, COURTNEY WEEKS, DAVID J. SERKE, AND ROELOF BRUINTJES

Using recent advancements in instrumentation and computer modeling, the SNOWIE project has observed the microphysical response from seeding orographic clouds and aims to address long-standing questions about using cloud seeding to enhance precipitation.

The need for water in arid regions around the world was recognized by pioneering scientists in the 1950s who, following the discoveries of

Schaefer and Vonnegut concerning cloud seeding (Schaefer 1946; Vonnegut 1947), developed projects, comprehensive for their day, to evaluate the scientific basis for weather modification as a tool to increase water supplies. These studies continued through the 1970s and '80s, and although they provided unparalleled advances in cloud physics understanding, they failed at their ultimate objective. In fact, enhancements in precipitation unambiguously attributable to cloud seeding have been nearly impossible to experimentally demonstrate (Kerr 1982; Garstang et al. 2003, 2005; Reynolds 2015). This is largely due to the difficulty in detecting what is assumed to be a relatively small signal (i.e., precipitation change as a result of cloud seeding) overlaid on a rather noisy field (i.e., variation in naturally occurring precipitation) either via statistics or direct measurement.

Part of the challenge in the early days was the inability of the available technology to measure the three-dimensional structure and composition of

AFFILIATIONS: TESSENDORF, RASMUSSEN, XUE, IKEDA, WEEKS, SERKE, AND BRUINTJES—NCAR, Boulder, Colorado; FRENCH, GEERTS, SNIDER, FABER, MAJEWSKI, GRASMICK, AND BERGMAIER—University of Wyoming, Laramie, Wyoming; FRIEDRICH AND AIKINS—University of Colorado, Boulder, Colorado; RAUBER, JANISZESKI, AND SPRINGER—University of Illinois at Urbana–Champaign, Urbana, Illinois; BLESTRUD, KUNKEL, AND PARKINSON—Idaho Power Company, Boise, Idaho
CORRESPONDING AUTHOR: Sarah A. Tessendorf, saraht@ucar.edu

The abstract for this article can be found in this issue, following the table of contents.

DOI:10.1175/BAMS-D-17-0152.1

In final form 2 August 2018

©2019 American Meteorological Society

For information regarding reuse of this content and general copyright information, consult the [AMS Copyright Policy](#).

clouds with sufficient accuracy and temporal and spatial resolution. In addition, relatively crude cloud parameterizations and computational limitations inhibited accurate numerical simulations of cloud and precipitation processes. However, recent advancements in instrumentation, better understanding of cloud dynamical and microphysical processes, and new and improved numerical modeling capabilities have laid the foundation to evaluate the potential of cloud seeding to enhance orographic precipitation in ways not possible in the past decades (Tessendorf et al. 2015). In this paper, we describe a comprehensive observational and modeling research project—Seeded and Natural Orographic Wintertime Clouds: The Idaho Experiment (SNOWIE)—that demonstrates a transformational approach to advance our understanding of orographic cloud dynamical and microphysical processes and addresses long-standing uncertainties regarding the effectiveness of orographic cloud seeding.

THE ORIGIN OF SNOWIE. SNOWIE developed during a renaissance in cloud-seeding research in the western U.S. states of Wyoming and Idaho. In the western United States, water and hydropower originates from snow deposited in the mountains in wintertime. In response to increased demands and limits on supplies, western communities have instituted water-conservation measures to preserve existing supply or have sought additional water sources through technologies such as cloud seeding (Kenny et al. 2009). Reduction of water supplies impacts the U.S. economy, reducing electricity generation (hydropower is a primary power source in the western United States), forcing agriculture to ration irrigation, affecting tourism, and threatening urban water supplies (Holmes 2012). It is worth noting that the problem of reduced snowpack is not limited to the United States (Chubb et al. 2011).

In response to rancher and farmer requests to evaluate the potential to use cloud seeding to enhance snowpack, and subsequent streamflow from snowmelt, the Wyoming Weather Modification Pilot Project (WWMPP) was initiated in 2004. The key goal of the WWMPP was to evaluate whether seeding orographic clouds from ground-based generators with a glaciogenic aerosol material [silver iodide (AgI)] could increase snowpack in critical water basins. The WWMPP included a randomized statistical experiment for six winter seasons aimed at providing a statistically significant estimate of the impact of cloud seeding over two similar mountain ranges in Wyoming (Breed et al. 2014). Despite a

novel statistical design, the experiment was inconclusive given that it was unable to detect a statistically significant result, yet it led to the development of new methods and tools for evaluating cloud seeding (Rasmussen et al. 2018).

In collaboration with the WWMPP, scientists initiated a National Science Foundation (NSF)-funded project, called AgI Seeding Cloud Impact Investigation (ASCII; Geerts et al. 2013), to investigate the likely impact of AgI seeding on targeted cloud systems using airborne and ground-based radars. ASCII took place during the WWMPP over the same mountain ranges but focused on storms that were seeded separately from the randomized statistical experiment. The ASCII case studies (Pokharel et al. 2014a,b; Chu et al. 2014, 2017a,b; Aikins et al. 2016) and composite studies (Jing et al. 2015; Jing and Geerts 2015; Jing et al. 2016; Pokharel and Geerts 2016; Pokharel et al. 2017) suggested an increase in radar reflectivity and precipitation from cloud seeding, but none of the ASCII cases showed a clearly delineated enhancement of radar reflectivity downwind of the AgI releases. Both ASCII and WWMPP focused on ground-based seeding, in which AgI was released at ground level using generators that burn an AgI solution and rely on turbulence and orographic flows close to the ground to disperse the seeding material into clouds with supercooled water. Because of this, the pattern of AgI dispersion is complicated and often remains close to the ground, making it hard to distinguish seeded from natural precipitation patterns. Moreover, it was impossible, because of safety reasons, for the ASCII research aircraft to collect measurements directly in the cloud regions containing the seeding material to evaluate the physical connection between seeding and cloud microphysical evolution. However, ASCII demonstrated the usefulness of the profiling airborne W-band Wyoming Cloud Radar (WCR) and scanning Doppler on Wheels (DOW) dual-polarization X-band radar to document the finescale details of orographic clouds in a manner that was not possible even 10 years ago (Aikins et al. 2016). This demonstrated that modern-day instrumentation had the capability to measure the impacts of cloud seeding in orographic clouds in a way not possible in earlier decades.

The other major advance propelled by the WWMPP was the use of high-resolution cloud models to evaluate cloud seeding. As part of the operational guidance needed for the WWMPP, the National Center for Atmospheric Research (NCAR) developed a regional real-time forecasting model to aid forecasters in determining when to seed. Additionally, NCAR led the development of

a cloud-seeding parameterization in the Weather Research and Forecasting (WRF) Model (Xue et al. 2013a,b) to simulate the impacts of cloud seeding. Part of the motivation for this development was the recent demonstration that high-resolution WRF simulations could accurately estimate seasonal snowfall and snowpack over the headwaters of the Colorado Rockies (Rasmussen et al. 2011). This result suggested that if the model could accurately simulate precipitation over complex terrain, then perhaps with the additional cloud-seeding parameterization, it could also simulate the impact of orographic cloud seeding.

Concurrent with the WWMPP, Idaho Power Company (IPC) was operating a cloud-seeding program in southern Idaho to augment snowpack, which is critical to their hydropower operations. IPC is an investor-owned utility serving over half a million customers in southern Idaho and eastern Oregon, and about half of the electricity delivered to IPC's customers comes from its 17 hydroelectric projects along the Snake River and its tributaries. Historically, IPC evaluated its cloud-seeding program using a target-control analysis, a commonly employed statistical technique (Dennis 1980). After seeing results of initial model simulations of cloud seeding, IPC water managers began collaborating with NCAR scientists to develop methods to use this modeling approach to provide physically based evaluation to supplement the statistically based target-control analysis they were conducting. The result was the initiation of a project to use cloud models to evaluate as well as forecast the possibility of cloud seeding in Idaho.

While the ability of the WRF Model to reproduce seasonal snowfall and snowpack has been demonstrated (Rasmussen et al. 2011; Liu et al. 2016), the ability of the cloud-seeding parameterization in WRF to accurately simulate the effect of cloud seeding on



FIG. 1. Photos of (a) the UWKA aircraft (courtesy L. Oolman, University of Wyoming) and (b) the DOW-7 radar located at Packer John at sunset (courtesy J. Aikins, University of Colorado Boulder).

clouds and precipitation has not. This led to a collaboration between IPC water managers, NCAR, and scientists from several universities to conduct a physically based cloud-seeding field program in Idaho to evaluate the modeling capability and to understand the science of orographic cloud seeding. The motivation was to combine state-of-the-art observational instrumentation with high-resolution modeling and the AgI cloud-seeding parameterization to study the physical chain of events of orographic cloud seeding in unprecedented detail. The experiment relied on a close collaboration with the IPC operational cloud-seeding program that targets the mountainous regions of the Payette basin in west-central Idaho. As a result, the NSF-funded SNOWIE field campaign was conducted 7 January–17 March 2017 in the Payette basin of Idaho. A unique aspect of SNOWIE was that it was composed of both privately funded (i.e., IPC) and publicly funded (i.e., NSF) research equipment and scientists, which was mirrored by the objectives of the project being relevant to both private and public interest.

TABLE 1. Measurements from the UWKA and WMI seeding aircraft.

| Class of measurement | Measure | UWKA instrument | WMI aircraft instrument |
|---------------------------------------|--|---|--|
| Atmospheric state | Pressure | Rosemount 150I high-accuracy digital-sensing (HADS) static pressure | Aircraft-Integrated Meteorological Measurement System (AIMMS) 20 pressure sensor |
| | Winds | Rosemount 858J 5-hole gust probe, Applanix POS AV coupled inertial navigation system (INS)–GPS | AIMMS 20 |
| | Temperature | Reverse-flow housing with platinum resistive element | Rosemount 102AUIAP total temperature sensor |
| | Water vapor | EdgeTech 137 Vigilant chilled-mirror hygrometer Licor LI-7000 closed-path infrared absorption analyzer | EdgeTech 137 Vigilant chilled-mirror hygrometer AIMMS 20 Humicap to measure relative humidity |
| In situ cloud properties | Bulk condensed water substance | Droplet Measurement Technologies (DMT) liquid water content (LWC)-100 hot-wire probe | DMT LWC-100 hot-wire probe |
| | | Gerber particle volume monitor (PVM) | DMT Cloud, Aerosol, and Precipitation Spectrometer (CAPS) hot wire |
| | | Nevzorov hot-wire probe | — |
| | Cloud hydrometeor size and concentration | Rosemount icing probe | — |
| | | DMT cloud droplet probe (CDP) | DMT CDP |
| | | Stratton Park Engineering Company (SPEC), Inc., optical array probe (OAP) two-dimensional stereo (2DS) | DMT OAP CIP as part of CAPS probe |
| Remotely sensed cloud properties | W-band equivalent radar reflectivity factor | WCR | — |
| | | | — |
| | Near-vertical W-band Doppler velocity | — | |
| | Ka-band equivalent radar reflectivity factor | Ka-band profiling radar (KPR) | — |
| | Attenuated backscattered power at 355 nm | WCL | — |
| Linear depolarization ratio at 355 nm | — | | |

EXPERIMENTAL DESIGN. The SNOWIE project was designed to investigate the impact of cloud seeding in the context of natural orographic precipitation processes, focusing on ice initiation, snow growth, and the impacts of orography on the development of precipitation. The primary scientific objectives of SNOWIE are 1) to evaluate the role of dynamical and microphysical processes that form and enhance clouds and precipitation and the impact of terrain on the formation, growth, and fallout of ice crystals in winter storms and 2) to describe and quantify the impact of airborne and ground-based

glaciogenic seeding¹ on hydrometeor growth processes and precipitation in wintertime orographic clouds. The information gained from the second objective will be used to evaluate and improve the AgI cloud-seeding parameterization (Xue et al. 2013a,b).

To meet these objectives, in situ and remote sensing measurements were collected with the University of Wyoming King Air (UWKA) research aircraft (Fig. 1a) prior to, during, and after seeding, with the goal of obtaining direct measurements within

¹ Via the static mode of cloud seeding.

seeded clouds and tracking effects of the seeding to the ground. The seeding opportunities were identified collaboratively between IPC forecasters and SNOWIE investigators based upon the forecast temperatures and winds, as well as the likelihood of supercooled liquid in clouds. If there was the potential for seeding, an intensive observing period (IOP) was declared, and seeding was performed² without any randomization procedure.

The UWKA research aircraft was equipped with a suite of instruments (Table 1), including cloud physics probes, liquid water content sensors, and remote sensing tools, such as the W-band WCR and Wyoming Cloud Lidar (WCL; Wang et al. 2012). In SNOWIE, AgI was released primarily from a seeding aircraft in order for the seeding material to disperse at an altitude that would allow for direct measurements by the research aircraft. The seeding aircraft, a Beechcraft King Air B200 operated by Weather Modification International (WMI), carried up to 24 burn-in-place (BIP) flares and 306 ejectable (EJ) flares per mission (Fig. 2). The BIP flares were ignited individually and sequentially, typically burning for about 4.5 min and releasing 16.2 g of AgI per flare to produce a continuous and nearly linear plume of AgI. The EJ flares emit 2.2 g of AgI per flare and were released roughly every 30 s, burning for about 35 s as they fall, which produces a semivertical line of AgI over a depth of about 820 m (2,700 ft) below flight level (Fig. 3). The type of flares used followed IPC's operational procedures, typically based upon whether the seeding aircraft was in cloud (BIP or BIP and EJ used) or above cloud (only EJ used). The King Air B200 seeding aircraft was equipped with an M300 data system and temperature and liquid water sensors, as well as particle size measuring probes (Table 1).

² Exceptions to this are that IPC does not seed when certain environmental criteria are met that could lead to hazardous situations. When such "suspension criteria" were met, no seeding was performed.



FIG. 2. Photos of (a) the WMI seeding aircraft, with close-ups of (b) instruments mounted under the wing and (c) the wing-mounted BIP flare rack with one BIP flare lit during seeding. (Photos courtesy of A. Brainard, WMI.)

For a typical IOP, the UWKA took off 30 min before the seeding aircraft in order to conduct at least one full flight leg parallel to the mean flight level wind prior to the onset of seeding with the seeding aircraft (Figs. 3, 4). The first leg was designed to collect measurements that would be used to characterize natural cloud conditions and to investigate the spatial heterogeneity in the absence of seeding. After the seeding aircraft took off, it would release seeding material as it passed back and forth along a track perpendicular to the prevailing wind direction upwind of the Payette basin. Immediately upon release, the seeding material would begin to disperse downwind of the aircraft track. While the aircraft flew back and forth along a straight track, the AgI dispersed in a zigzag pattern as it (and any potential ice particles created from it) was transported downwind (Fig. 3). During this time, the UWKA would continue flight legs along the wind direction, back and forth along the same track over the Payette, crossing through the zigzag AgI plume pattern (Fig. 3). Typical flight times for the seeding aircraft were 1–2.5 h, while the UWKA was on station for up to 3.5 h per IOP (typically 10–14 flight legs). After the seeding aircraft completed seeding (typically 2–8 flight legs), the UWKA continued flight legs back and forth over the Payette basin to observe further evolution of seeded clouds.

While the focus of SNOWIE was on airborne seeding, ground-based seeding was performed as

part of the IPC operational cloud-seeding program and during three SNOWIE IOPs. Ground-based seeding cases utilized 12 remotely operated

generators located along the upwind ridges of the Payette basin (Fig. 4). These ground-based generators typically released 20 g of AgI per hour.

To provide three-dimensional context for the aircraft measurements, two dual-polarization DOW mobile X-band radars (Fig. 1b) were sited at fixed locations atop mountain ridges (Packer John and Snowbank) upwind of the Payette basin (Fig. 4). The DOW radar located at Packer John focused on scanning range-height indicator (RHI) scans in high temporal resolution parallel to the wind direction. The UWKA flight tracks were designed to intersect the Packer John DOW site while flying parallel to the prevailing wind direction. Therefore, the RHI scanning strategy from Packer John provided updates every 30 s to monitor fast-evolving processes, in particular, the impact of airborne seeding on snow growth and natural orographic precipitation processes, along the flight track of the UWKA. The DOW radar located at Snowbank provided 360° volume scans to monitor the microphysical information and mean wind profile within the storms. DOWs operated 2 h prior to the takeoff of the UWKA until 2 h after the UWKA landed. Each of the DOW sites served as principal instrument sites that included several other instruments, such as a vertically pointing Ka-band Micro Rain Radar (MRR; Löffler-Mang et al. 1999; Aikins et al. 2016), an OTT Particle Size Velocity

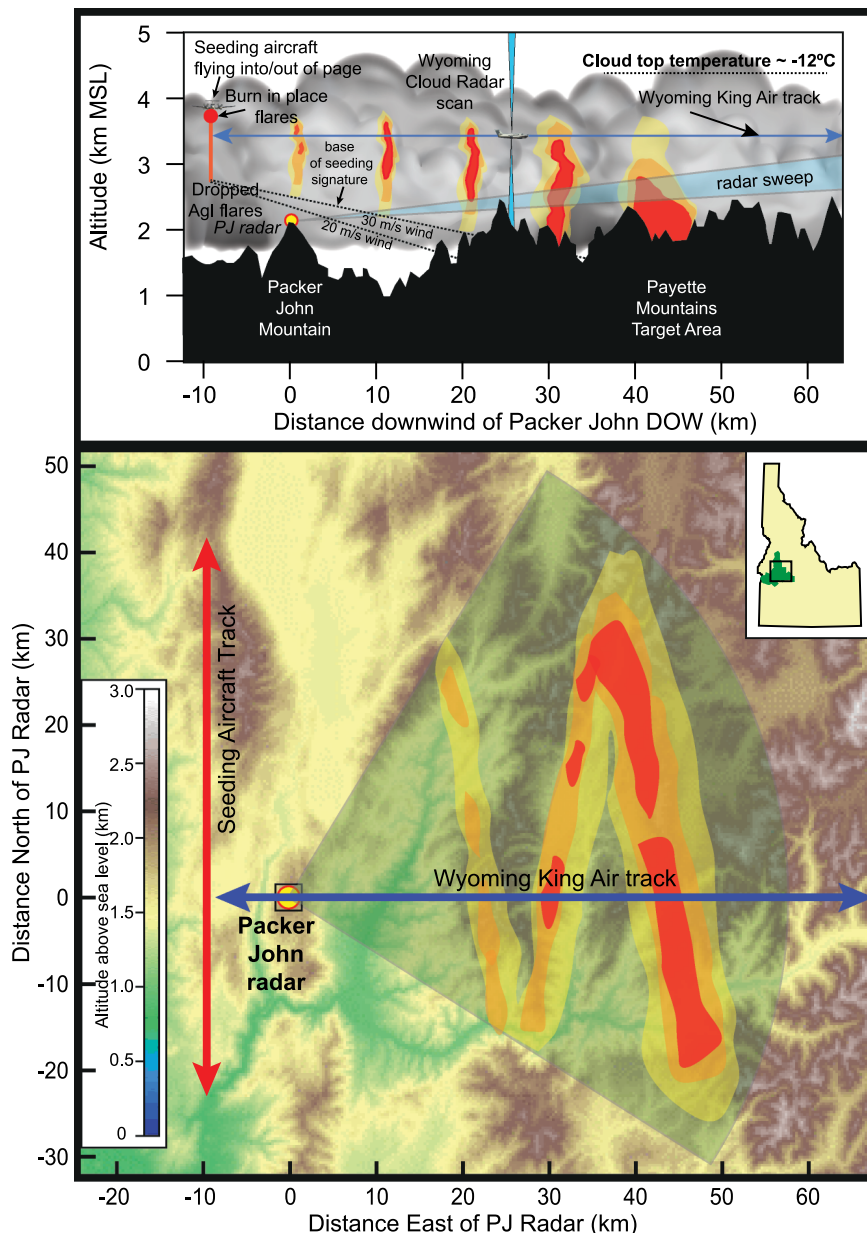


FIG. 3. A conceptual illustration of the anticipated seeding signature and the experimental setup as part of SNOWIE. The yellow–orange–red colors indicate locations and relative magnitude of radar reflectivity echoes. Yellow dots show locations of ground-based radars, the red line represents a typical flight track for the seeding aircraft under westerly winds (left to right across the figure), and the blue line is the corresponding flight track for the UWKA. (top) A vertical cross section along the flight track of the UWKA and (bottom) a plan view. Seeding material is released either as BIP or EJ flares. Vertical depth of echoes as a function of downwind distance depends, in part, on wind speed. The bases of the radar echo descend as particles grow and fall and are illustrated by the dashed lines in the top panel for two different wind speeds. Here, for illustration purposes, we assume constant wind speed with height. [Figure from French et al. (2018).]

(PARSIVEL) disdrometer (Löffler-Mang and Joss 2000; Friedrich et al. 2016), and surface meteorological observations. MRRs provide vertical profiles of reflectivity and Doppler velocity every minute, while the disdrometer provides particle sizes and fall velocity at the surface.

A network of 12 high-resolution Geonor, Inc., snow gauges were deployed in the Payette basin target area to measure the snowfall with high temporal frequency and to less than 1-mm resolution. Four gauge sites were located along the upwind ridge, either collocated or upwind of ground-based AgI generators, while the remaining eight high-resolution snow gauge sites were sited within the Payette basin (Fig. 4). Five of the gauge sites within the Payette basin utilized high capacity (3,000 mm) T-200B systems, while the remaining seven gauge sites utilized standard capacity (1,500 mm) T-200B systems. Two of the Payette basin snow gauge sites included both a Geonor (1,500 mm) T-200B and an Electronic Temperature Instruments (ETI) Instrument Systems, Inc., NOAH II snow gauge. Having two gauges at each site provides redundant measures to aid in quality control analysis. Snowpack Telemetry (SNOTEL) gauges, operated by the Natural Resources Conservation Service, are also located around the Payette basin and provide long-term measurements of precipitation in the region; however, their measurement resolution is only 2.5 mm.

Six scanning microwave radiometers manufactured by Radiometrics Corporation (Solheim et al. 1998; Ware et al. 2003) were located along the upwind ridge and into the Payette basin in order to measure liquid water path in the clouds (Fig. 4). Four of the units were multichannel Microwave Profiler (MP)-3000 models, while the other two were dual-channel [Water Vapor Profiler (WVP)-1100 and WVP-1500] models. Three rawinsonde units were used to measure temperature, relative humidity, and wind profiles during IOPs (Fig. 4). At least one rawinsonde was launched 2–4 h prior to launching the UWKA, and the data were used to determine whether to continue with a planned IOP. Once the UWKA was airborne, rawinsondes were launched regularly every 1–2 h, rotating through the three rawinsonde sites to sample across the region of interest. A fourth rawinsonde unit that included a vibrating wire instrument (Serke et al. 2014) to measure profiles of supercooled liquid water content was available in some IOPs. These special sondes were launched from the Horseshoe Bend site collocated with one of the scanning MP-3000 microwave radiometers.

Two ground-based in situ aerosol measurements provided information about aerosol concentrations and ice nucleating particle (INP) concentrations. A

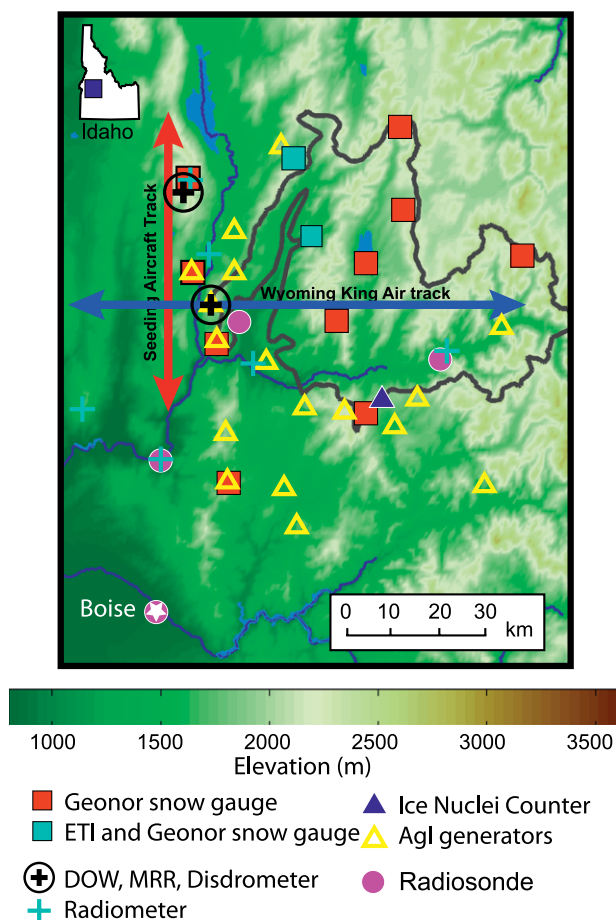


Fig. 4. Terrain map of the SNOWIE project domain north of Boise illustrating the sites of ground-based instrument locations (see legend) as well as an example flight track for the seeding aircraft and UWKA, assuming conditions with westerly winds. The Payette River basin, outlined in thick gray, was the target region for the SNOWIE field campaign. The northern DOW radar was located at Snowbank, and the southern DOW radar was located at Packer John.

passive cavity aerosol spectrometer probe (PCASP; Strapp et al. 1992) was located at the Snowbank DOW site, and an acoustic ice nucleus counter (AINC; Langer 1973) was located along the southern boundary of the Payette basin (Fig. 4). No direct measurements of cloud condensation nuclei (CCN) or the full spectrum of INP were included in the field campaign, however. The AINC detects INP that activate at temperatures warmer than -20°C and therefore is useful for detecting AgI INP used for cloud seeding (Super and Huggins 1992; Jing et al. 2016). It has been used in previous cloud-seeding experiments in Colorado and Wyoming to infer the presence of AgI when concentrations exceed background levels measured prior to the onset of seeding (Super and Boe 1988; Boe et al. 2014).

Working in conjunction with IPC, the Boise State University Department of Geosciences Trace Chemistry Laboratory collected snow samples both in real time and after the event (the latter were column samples collected by digging snow pits) within the Payette basin to be analyzed for trace amounts of silver.³ These analyses will be used to compare both the spatial and temporal distribution of silver in the snow with model simulations using the cloud-seeding parameterization following similar methods as in Xue et al. (2017).

SNOWIE data are publicly available for all researchers and can be obtained on the Earth Observing Laboratory (EOL) data archive (<http://data.eol.ucar.edu/masterlist/?project=SNOWIE>).

OVERVIEW OF THE CLOUDS AND PRECIPITATION DURING SNOWIE. During the 10-week field campaign, 24 IOPs were conducted,⁴ 23 of which included a UWKA research flight.⁵ Based on a climatological assessment of the region performed prior to proposing the program, it was anticipated that 15–20 IOPs could be expected during the 10-week campaign. Fortunately, the weather pattern was very active during SNOWIE and led to more IOPs than originally planned, as well as a wide variety of winter storm conditions. In fact, the precipitation accumulation during the campaign was in the 95th percentile of winter precipitation accumulation over the past 30 years, resulting in the second wettest winter during this period (Fig. 5). Interestingly, the precipitation accumulation at the beginning of the campaign was quite normal, in line with the 30-yr median, yet during the course of the

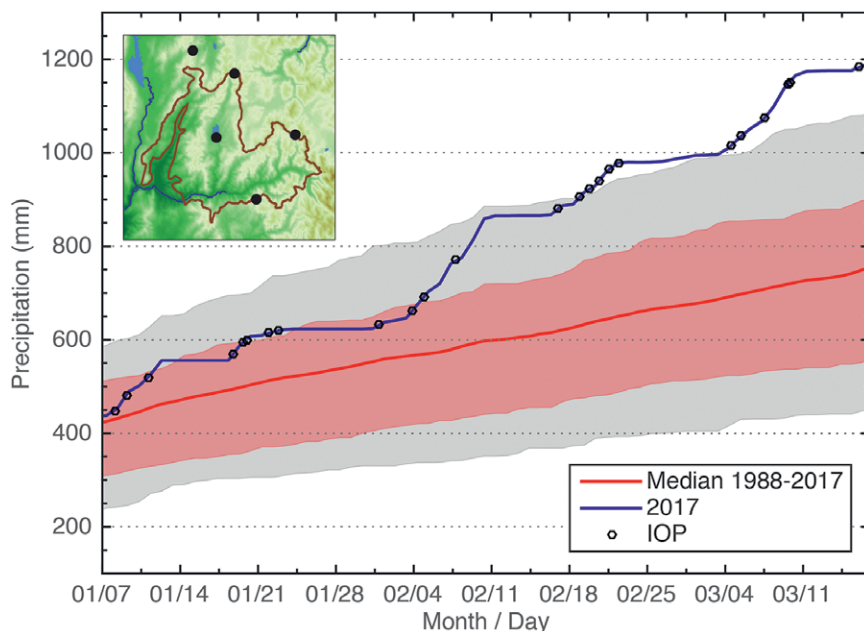


Fig. 5. Area average (liquid equivalent) precipitation gauge accumulation (mm) from five Snowpack Telemetry (SNOTEL) sites in the Payette basin study region (see black dots on inset map) for the SNOWIE campaign period starting 7 Jan through 17 Mar 2017 (blue line) compared to the 30-yr statistics for the same period from 1988 to 2017. The statistics from the area average precipitation accumulation over the 30-yr period include the median (red line), the 25th–75th-percentile region (red shading), and the 10th–90th-percentile region (gray shading). Black open circles along the 2017 accumulation line represent when SNOWIE IOPs occurred.

campaign, several storms impacted the area that led to anomalously high snowfall accumulation, as well as some local and regional flooding. For full clarity, we should mention that unusually heavy snow was measured not only in the Payette basin target area but also in other unseeded areas nearby; in other words, Fig. 5 is not intended to imply any seeding impact. Because the precipitation accumulation was so much greater than normal, the seeding aspect of SNOWIE was suspended on 7 March 2017, leaving the remaining flight hours to focus on natural cloud missions. During the last three IOPs (IOP 22–24), dual-aircraft research missions were flown, utilizing the seeding aircraft as a second research aircraft that flew along the same flight track as the UWKA, 2,000 ft below. Since natural cloud studies are a critical part of meeting the SNOWIE objectives, these IOPs provide data with a unique sampling

³ See Fisher et al. (2018) for more details on the snow sampling procedures and associated analysis. Snow sampling data from SNOWIE are preliminary and will be published in future manuscripts.

⁴ Mission summaries can be found on the SNOWIE Field Catalog (<http://catalog.eol.ucar.edu/snowie>).

⁵ No UWKA flight occurred during IOP 18 because favorable conditions dissipated before takeoff, so the UWKA flight was canceled, yet DOW data were collected.

strategy compared to the earlier IOPs and are useful for studying natural winter cloud microphysics.

To detect the impacts of cloud seeding from the natural background conditions, it is essential to understand the natural cloud structure and microphysical processes. One key observation from SNOWIE is that the natural clouds in this region are complicated, often exhibiting finescale structures and evolving characteristics. Clouds during IOPs were also quite diverse, including shallow and deep, stable and convective, and single-layer and multilayer clouds (Fig. 6). During the 23 IOPs that the UWKA flew, in situ measurements were collected in the $\sim -25^{\circ}$ to -5°C temperature range and spanned conditions that were liquid dominated, mixed phase, and ice dominated (Fig. 7). Precipitation accumulation during IOPs varied from very trace amounts to over a millimeter of liquid equivalent accumulation (Fig. 7). Sounding data from each IOP indicated that temperatures at 700 hPa, approximately the height of the highest mountains along the eastern border of the Payette basin (i.e., the Sawtooth Range), were relatively warm for winter storms, ranging from -1° to -14°C . Moreover, the 700-hPa wind speeds for each IOP ranged from weak (5 m s^{-1}) to strong (27 m s^{-1} ; Fig. 7). The range of the mean vertically integrated liquid

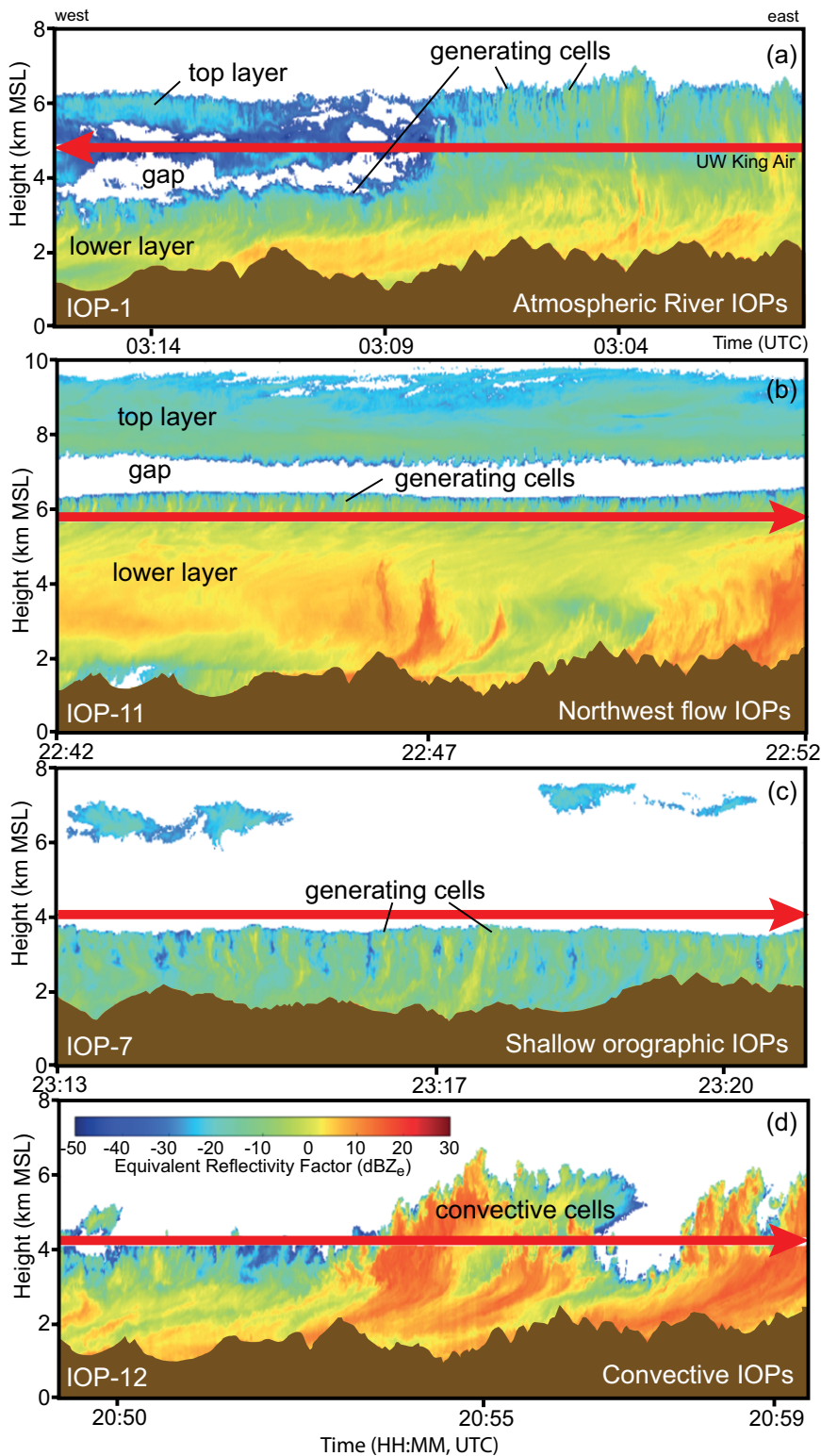


FIG. 6. West–east cross sections across the Payette Mountains showing the equivalent radar reflectivity factor from the WCR illustrating the cloud structure during four weather patterns observed during SNOWIE: (a) IOP 1, (b) IOP 11, (c) IOP 7, and (d) IOP 12. The red line shows the UWKA flight level and direction. West is on the left on all panels.

water path (LWP) observed by the Horseshoe Bend radiometer during each IOP varied from very little for some IOPs to near 1 mm or greater, such as in IOP 9 and IOP 24 (Fig. 7). Note that IOP 18 had negligible mean LWP, which is why no UWKA flight occurred in this case.

The sounding data also revealed that the low-level flow was usually blocked given that the Froude number (Fr) calculated between the upwind Snake River Plain and the mean height of the Sawtooth Range (downwind of the Payette basin) was generally below unity (Fr < 1; Fig. 8). This is in contrast with the ASCII campaign in Wyoming, where 85% of the IOPs had (deep layer) Fr values > 1 (Pokharel and Geerts 2016). This flow trapping usually was confined to the lowest levels, below the height of Packer John Mountain on the western border of the Payette. The Froude number in the upper-layer air (above Packer John's elevation but still below the Sawtooth Range crest) was much higher, typically >1, indicating that this air mass was more freely lofted over the mountain barrier (Fig. 8). This agrees with the general observation during SNOWIE that

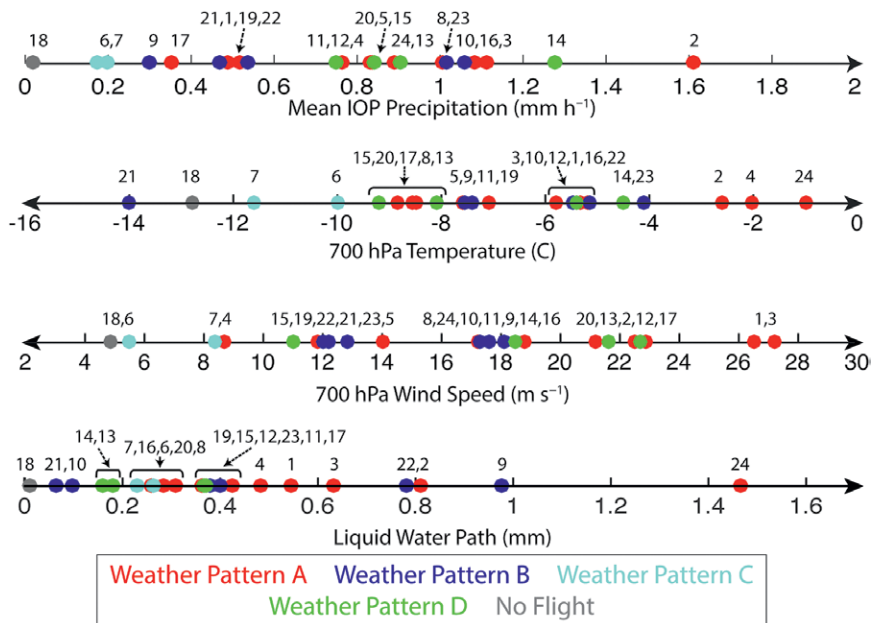


FIG. 7. Distributions of various metrics observed during SNOWIE IOPs: mean precipitation accumulations during IOPs were averaged across available Geonor gauge sites in the SNOWIE domain, 700-hPa temperature and wind speed were observed by soundings released at Crouch, and mean LWP observed by the Horseshoe Bend radiometer during IOPs (missing for IOP 5). Each dot represents an IOP (with the IOP numbers labeled above each) and are color coded to match the synoptic weather patterns illustrated in Figs. 6 and 9.

orographic precipitation was generated in a cloud layer decoupled from the near-surface layer in the upwind basin. The shallow air mass near the surface was generally cold, especially in the first half of the campaign, essentially a Snake River Plain drainage current around the Idaho central mountains (Steenburgh and Blazek 2001). The flow in the upper layer, on the other hand, was mostly from the southwest, originating over the Pacific Ocean.

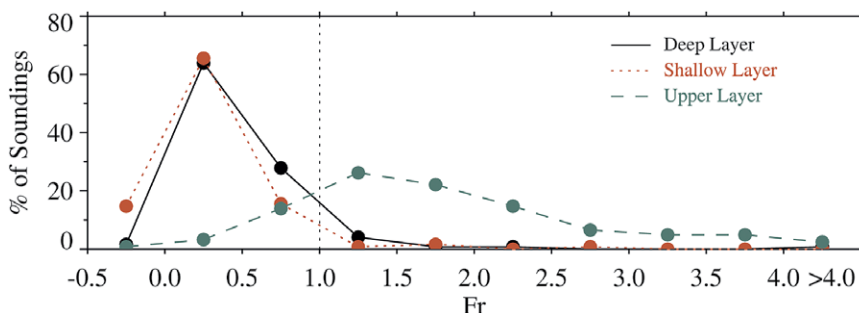


FIG. 8. Histogram of Froude number (Fr) calculated using all soundings launched at Crouch ± 4 h of an IOP. Three layers (H) were assessed: a traditional deep layer defined with $H = 1,868$ m, from the height of the surface (1,082 m MSL) to the mean height of the Sawtooth Range east of the Payette basin (2,950 m MSL), as well as for a shallow layer defined with $H = 1,082$ m, from the height of the surface (1,082 m MSL) to the height of Packer John DOW radar (2,164 m MSL), and an upper layer was defined with $H = 786$ m, from the height of Packer John to the mean height of the Sawtooth Range (2,950 m MSL). (Note that the boundary normal wind was used in this calculation, which occasionally resulted in slightly negative Fr when flow away from the mountains occurred.)

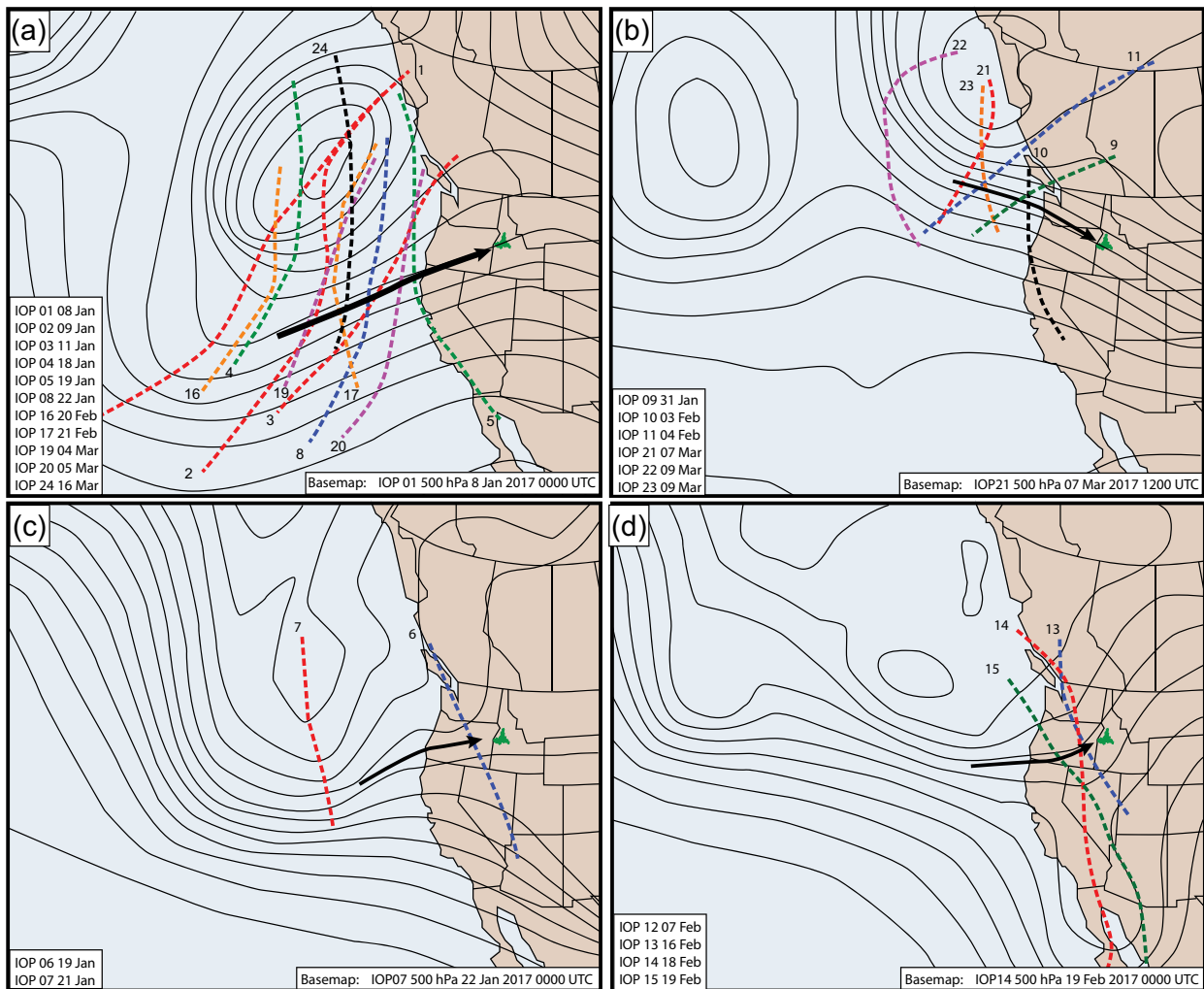


FIG. 9. The 500-hPa height fields near the times of UWKA flights for (a) IOP 1, (b) IOP 21, (c) IOP 7, and (d) IOP 14. The green area in Idaho denotes the Payette basin. The dashed lines denote trough positions for the IOPs listed in the tables within each panel, with the number at the end of each line indicating the IOP. The four weather patterns are described as (a) atmospheric river events, (b) northwest flow events, (c) orographic cloud events, and (d) convective cloud events. The black arrows denote the flow direction in the Payette region at the 500-hPa level.

Common weather patterns. The dominant weather pattern (11 IOPs) during SNOWIE was associated with atmospheric river (AR) events off the Pacific Ocean (Zhu and Newell 1998; Ralph et al. 2017), many of which exhibited multiple cloud layers. Synoptic characteristics of these IOPs were a deep 500-hPa trough off the west coast, a ridge east of Idaho, and southwesterly flow directed into the Payette Mountains east of the trough. The position of the trough axis varied, but the common characteristic was a deep band of moist air flowing from the Pacific across the Sierra Nevada/Cascade Range and over the Payette basin (Fig. 9a). Figure 6a shows WCR data from an east–west pass of the UWKA across the Payette. Note two cloud layers on the west side of Fig. 6a. This split

layer characteristic was observed during all or part of 9 of the 11 AR IOPs, while 2 IOPs had consistently deep clouds. During the nine IOPs, the upper cloud layer sometimes merged with the lower layer (e.g., east side of Fig. 6a) while at other times remained completely distinct with no radar echo present in the gap. From satellite imagery, upper cloud layers were a continuation of upper-tropospheric ascent into the Payette, while lower cloud layers appeared to be forced by low-level ascent over the Payette. Mergers occurred when ice precipitated from the upper into the lower layer, effectively seeding the lower layer. Ice-generating cells (see Keeler et al. 2016a,b, 2017, and references therein) were observed at the top of the lowest layer in all AR IOPs and at the top of the upper

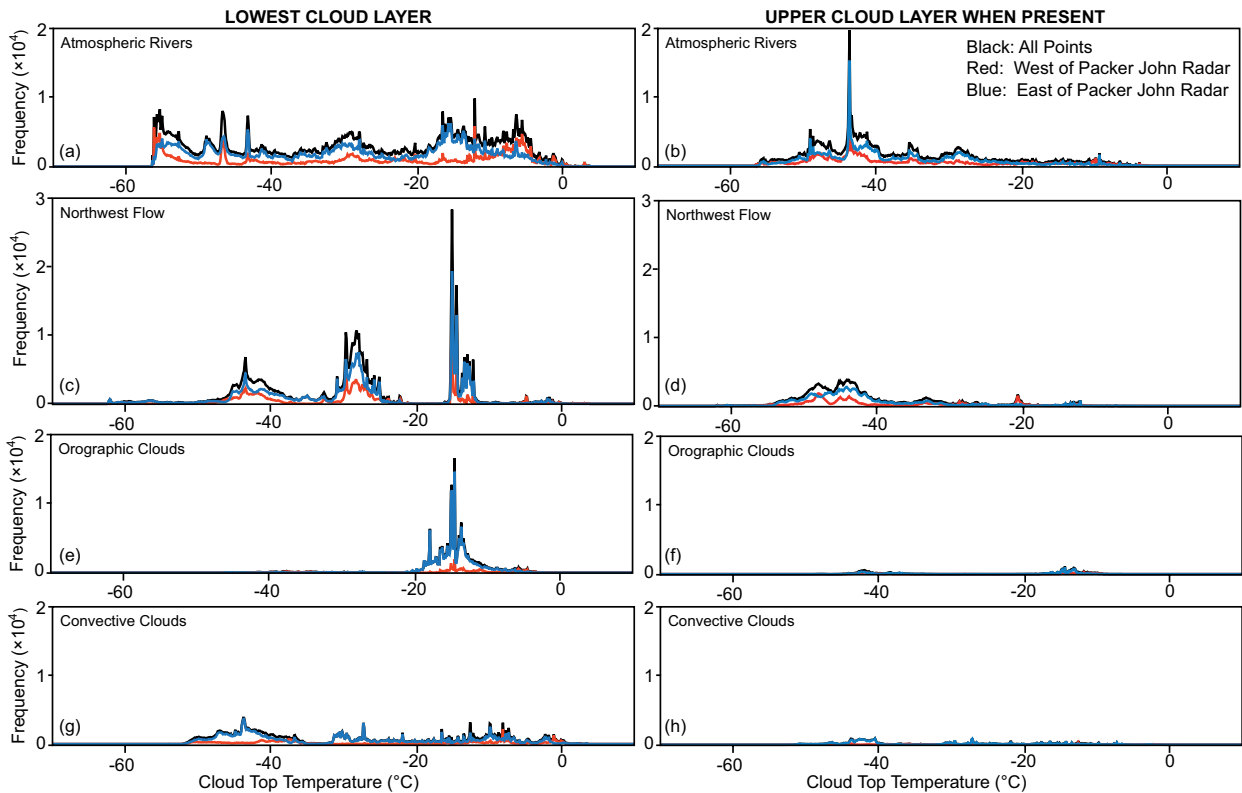


FIG. 10. Cloud-top temperature statistics derived from equivalent radar reflectivity factor measurements from the WCR and project soundings for (a),(c),(e),(g) the lowest cloud layer and (b),(d),(f),(h) upper cloud layer when present during (a),(b) atmospheric river, (c),(d) northwest flow, (e),(f) orographic cloud, and (g),(h) convective cloud events. The frequency of occurrence of such upper cloud layers is shown as a percentage below each synoptic type in (b), (d), (f), and (h). The WCR cloud-top height was expressed in terms of temperature using a proximity sounding (the closest-in-time Crouch sounding).

layer in 7 of 11 AR IOPs. The temperatures at the top of the lowest cloud layers ranged from 0° to -55°C (Fig. 10a). Note the frequent occurrence of lower cloud-layer cloud-top temperatures between -6° and -17°C in AR events, conditions considered suitable for seeding (Grant and Elliott 1974). Updrafts associated with generating cells, together with warm cloud-top temperatures, often led to the existence of supercooled water near the cloud top of the lower layer during these conditions, again providing suitable conditions for cloud seeding. The mode of cloud-top temperatures around -15°C was primarily from clouds observed over the mountains, while the warmest mode of -6°C was primarily from clouds over the upwind plain west of Packer John. This is consistent with the Fr calculations that low-level air over the upwind plain was often blocked by the mountains, so clouds that formed in this low-level air mass often remained quite shallow (Fig. 8). Figure 10b shows the temperatures at the top of the upper layer when two layers were present. These clouds typically had tops colder than -30°C and were a source of natural ice from aloft.

The second common pattern (six IOPs) during SNOWIE was a trough embedded in northwest flow (NF; Fig. 9b). Half of the NF events had two cloud layers stretching across the Payette basin (Fig. 6b). Unlike the AR IOPs, these cloud layers remained separated during the flights. The other half (three events) had a single cloud layer. Temperatures at the top of the lower layer (or single layer) were cold in four of the NF IOPs, ranging from -20° to -62°C . Two had tops ranging from -10° to -18°C (Fig. 10c). One of these events exhibited ice-generating cells and supercooled water at cloud top. The other event did not, but supercooled water was present in the cloud. These two clouds had conditions suitable for seeding. The upper layer, when present, had cold cloud tops typically ranging from -30° to -55°C (Fig. 10d).

Two IOPs were characterized by shallow orographic clouds. One occurred prior to the arrival of deeper clouds associated with an AR event, while the other occurred after the departure of the deep clouds (Fig. 9c). Cloud-top temperatures ranged from -5° to -20°C during the flights (Fig. 10e),

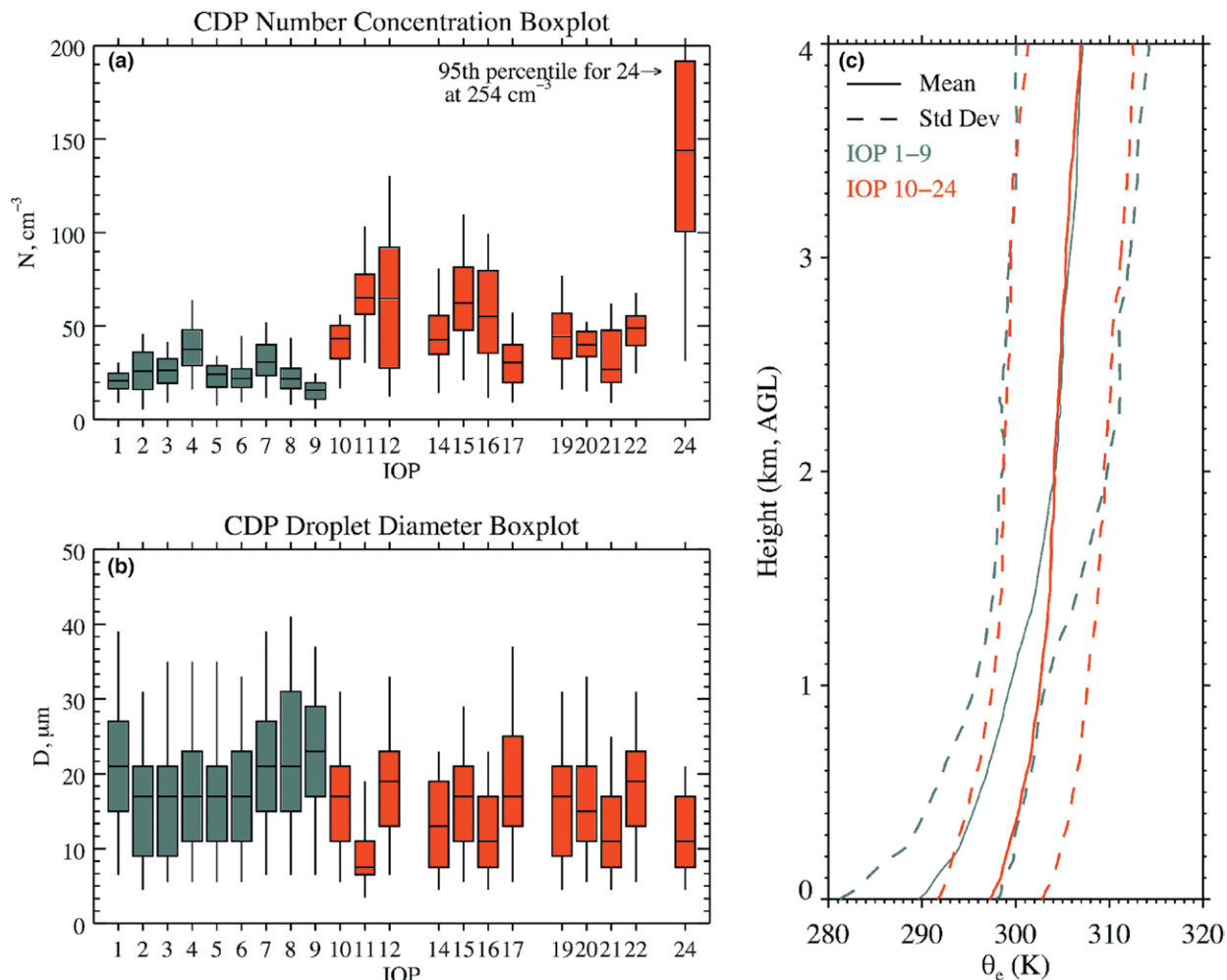


FIG. 11. (a) Box-and-whisker plots showing 5th, 25th, 50th, 75th, and 95th percentile for droplet number concentration N (cm^{-3}) and (b) droplet diameter D (μm) during periods containing only supercooled liquid water (without precipitation-size ice) over each flight. (c) Composite equivalent potential temperature q_e (K) profiles compiled over all IOPs. Graphs are color coded such that data from the first nine IOPs are shown in gray and data from the remaining IOPs are shown in red. IOPs 13 and 23 are not included because precipitation-size ice was always encountered when in cloud during those flights. No flight was conducted during IOP 18.

ice-generating cells were present at cloud top, and supercooled water was present at times when the aircraft was able to fly low enough to pass through the clouds (Fig. 6c). These clouds had conditions suitable for seeding. Overlying cloud layers were absent during these events except for a few passing cirrus clouds (Fig. 10f).

Four IOPs were associated with shallow to deep convection over the Payette. These events occurred as troughs, and associated cold air aloft, passed directly over the region (Fig. 9d). The convection produced strong winds and heavy graupel showers at the DOW sites and weak microburst outflows with occasional shelf clouds in the Snake River valley. Cloud tops in the cells rose to 6–8 km MSL (Fig. 6d). Cloud-top temperatures ranged from 0° to

-50°C as the cells approached and passed over the Payette (Fig. 10g). Targeted airborne seeding was more difficult in these conditions. Overlying cloud layers were largely absent (Fig. 10h).

Microphysical highlights. The frequent decoupling of the orographic cloud layer from the underlying surface led to surprisingly low concentrations of cloud droplets in the observed clouds. Figures 11a and 11b show the range of cloud droplet concentration N and diameter measured by the UWKA for each IOP. The data were compiled for regions containing few ($<0.5 \text{ L}^{-1}$) precipitation-sized particles, where radar reflectivity was less than -5 dBZ , in order to avoid regions where N may have been reduced by precipitation scavenging. Throughout the entire project, median

N was less than 70 cm^{-3} for all but the last IOP. Such low droplet concentrations have been observed along coastal mountain ranges of Oregon and Washington and over the Sierra Nevada in eastern California (Rauber 1992; Ikeda et al. 2007; Rosenfeld et al. 2013) attributed to low CCN from source air originating over the eastern Pacific. However, the study region for SNOWIE is more than 650 km from the ocean. Also, air arriving at the Payette under westerly flow must pass over the Treasure Valley, which includes the Boise–Nampa, Idaho, metropolitan area with a population of more than 600,000. One might expect that such a metropolitan area would serve as a notable source of aerosol and that under westerly flow conditions the aerosol, and hence cloud droplet populations, would be more continental in nature if the aerosol mix into the cloud layer. However, that was not the case for nearly all IOPs during SNOWIE. Therefore, it seems that there was little local influence of the aerosol population impacting the cloudy air over the Payette during SNOWIE.

Measurements from early IOPS (1–9) indicate significantly fewer cloud droplets compared to later IOPs (10–24), although even in most of the later IOPs, N is significantly less than typically observed in orographic clouds in the intermountain western United States (Politovich and Vali 1983; Rauber and Grant 1987; Borys et al. 2000). Composite soundings of equivalent potential temperature q_e shown in Fig. 11c indicate this earlier period contained notable stability in the lowest 2 km, consistent with low-level air being trapped in the valleys and decoupled from the

air flowing over the mountains, providing at least a partial explanation for the observations of low N . Not surprisingly, low values of N resulted in rather large droplet diameters, with median values of roughly $20 \mu\text{m}$ during an IOP and 95th-percentile values exceeding $35 \mu\text{m}$ in several cases. The development of such large droplets led to an active coalescence process and subsequent development of supercooled drizzle that was observed in numerous IOPs.

HIGHLIGHTS FROM CLOUD-SEEDING EXPERIMENTS.

Direct observations of ice production, growth, and fallout of precipitation due to seeding are exceedingly rare (Hobbs et al. 1981; Deshler et al. 1990; Deshler and Reynolds 1990). Part of this is due to the challenges with siting instruments and obtaining sufficient measurements in areas with complex terrain. During SNOWIE, the placement of the DOW radars on the upwind ridge was an operational and logistical challenge, yet it provided critical observations for detecting the impacts of seeding on precipitation. In addition, the conditions during several IOPs were favorable for the detection of seeding signatures—specifically, zigzag patterns of radar reflectivity visible in the DOW plan position indicator (PPI) scans. These signatures are associated with the dispersion of AgI released by the seeding aircraft, which leads to the initiation and growth of ice particles and also results in vertical descending reflectivity echoes on the WCR cross sections and DOW RHIs (Fig. 3). Indeed, detailed observations were collected illustrating the expected evolution

of cloud and precipitation particles following the nucleation of ice with AgI (French et al. 2018). Here, we present highlights from three IOPs in which ground-based and airborne remote sensors and in situ cloud instruments were used to detect and track seeding signatures embedded within the orographic cloud as they passed over the target region.

Figure 12 shows two PPI scans from the Packer John DOW radar from IOP 6; the first scan was taken approximately 1 h following the initiation of seeding and the second about 30

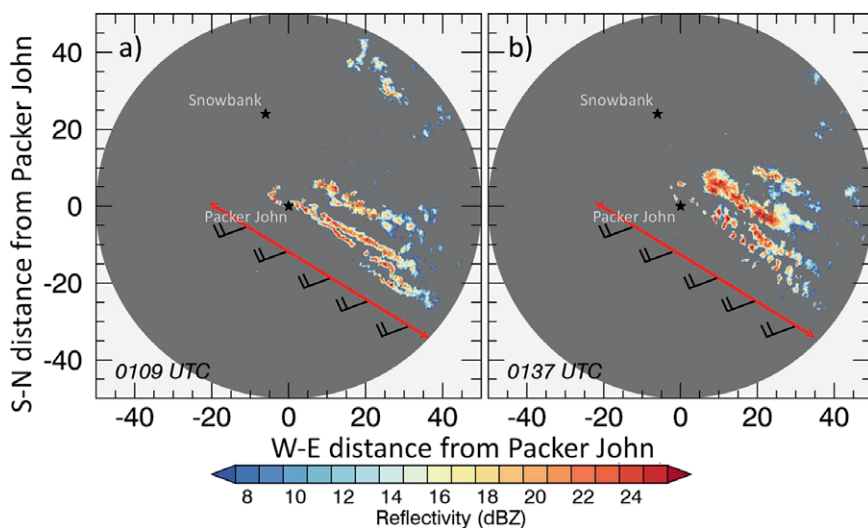


FIG. 12. PPI scans (0.99° elevation angle) at (left) 0109 and (right) 0137 UTC from the Packer John DOW radar. The red line denotes the track of the seeding aircraft. The track was repeated eight times between 0003 and 0129 UTC. The wind barbs indicate mean flight-level winds (kt; $1 \text{ kt} \approx 0.5144 \text{ m s}^{-1}$).

min later. Prior to seeding, the area was largely devoid of radar reflectivity echoes. About 30 min following the start of airborne seeding, radar echoes with reflectivity between 15 and 25 dBZ began to appear 10 km downwind of the flight track of the seeding aircraft. These echoes drifted with the environmental wind to the east-northeast, and the lines developed as hypothesized, following the zigzag pattern shown in Fig. 3. The seeding aircraft repeated its track for eight legs. Seeding began at 0000 UTC and continued until 0130 UTC. Flight legs were flown near the level of cloud top between 3.8 and 4.1 km MSL. All legs were seeded using EJ flares, and five of the legs were also seeded using BIP flares. For the legs seeded with EJ flares only, the emerging radar reflectivity lines appear dotted, with separation between reflectivity maxima of about 3 km, corresponding to the same separation as the EJ flare releases (Fig. 12b).

During IOP 5, the DOW radars and the WCR tracked two seeding lines, and the UWKA obtained measurements of the cloud particle phase and size distributions (Fig. 13) for seven flight legs over a period of 75 min. These data provide the first-ever observations of the detailed evolution of hydrometeor characteristics and precipitation development due to AgI seeding of orographic clouds (French et al. 2018). The seeding aircraft conducted six legs on two different tracks; however, only the first two legs (flown at 4 km MSL) were near enough to cloud top for the seeding material to make it into the clouds. Subsequent legs, flown at 4.5 km MSL as cloud tops on the upwind side were descending, were too high for the AgI to impact the clouds. Seeding began at 1620 UTC, and the second leg was completed by 1650 UTC. At

1730 UTC, the UWKA passed through two seeding lines: line A (B) roughly 18 (23) km downwind of the Packer John DOW (Fig. 13c). Radar reflectivity from the WCR in line A extended from cloud top, about 4.4 km MSL, to near the surface; in line B, which resulted from seeding about 15 min later than line A (see French et al. 2018), reflectivity echoes did not yet extend to the surface in the vertical plane viewed by the WCR. Values of reflectivity within the seeding lines were 10–30 dB greater than the immediate surrounding area. Hydrometeor size spectra collected at the flight level of the UWKA (~4 km MSL) indicate that, outside of the seeded regions, nearly all particles had diameters less than 100 μm and were composed mostly of liquid (dashed lines in Fig. 13b). However,

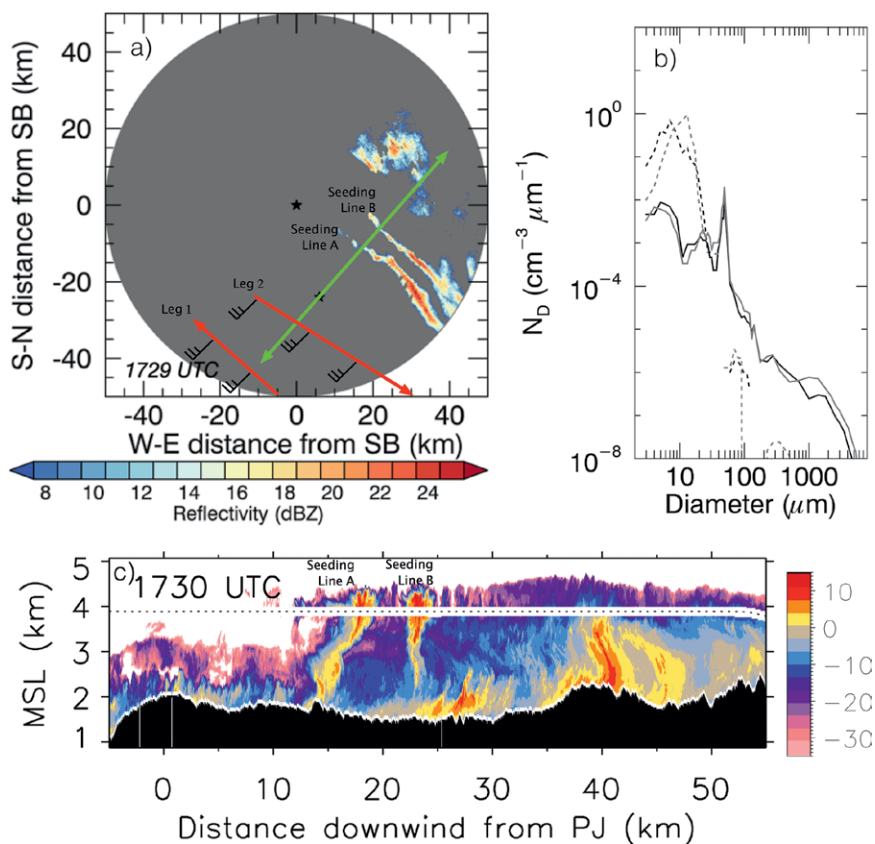


FIG. 13. Observations from several instruments during IOP 5. (a) PPI scan from the Snowbank DOW radar at 0.99° elevation angle and 1729 UTC. The red line denotes the track of the seeding aircraft. “Leg 1” results in seeding line A, “leg 2” in seeding line B. Wind barbs show mean flight-level wind (kt). The green line indicates the flight track of the UWKA. (b) Particle size distributions collected by cloud physics probes on the UWKA at 1730 UTC within the seeded regions (solid line; black: seeding line A; gray: seeding line B) and just outside of the seeded region (dashed lines). (c) Vertical profile of reflectivity from the WCR during a pass through the two seeding lines at 1730 UTC. The dashed line in (c) represents the flight level of the UWKA as the aircraft passed along the green line in (a). The black portion at the bottom of (c) is the underlying terrain. The track is plotted as distance downwind (to the northeast) of the Packer John radar, indicated by the star under the green line in (a).

inside of the seeded regions, rime ice particles and aggregates up to 4 mm in diameter were observed, and the cloud liquid water content had been reduced to near zero. French et al. (2018) describe the detailed evolution of the characteristics observed in the seeded regions over all seven of the UWKA flight legs in IOP 5.

Examples from a third seeding case, IOP 9, demonstrate the complexity associated with interpreting seeding signatures from the SNOWIE data. Two airborne tracks were seeded during this IOP between 2039 and 2105 UTC, one northbound leg and one southbound at 5 km MSL, both of which used BIP and EJ flares. During this case, winds near cloud top at 5 km MSL were out of the west at 45 m s^{-1} and decreased to 20 m s^{-1} at 3 km MSL. The large amount of shear resulted in radar reflectivity echoes from the DOW PPI scan that showed a significant horizontal displacement between the more continuous echo line generated from BIP flares and the separated echoes from EJ flares despite both

being released along the same seeding flight leg (Fig. 14a). At nearly the same time as the PPI scan, the UWKA passed over and just through the top of an EJ seeding signature at the very top of the cloud, about 7 km downwind of Packer John. Vertical profiles from the WCR indicate very thin, narrow lines of enhanced radar reflectivity that demonstrate extreme tilt due to the vertical wind shear (Fig. 14c). Measurements from cloud physics probes on the UWKA obtained at cloud top indicate that, outside of the line, hydrometeors were all liquid and had a mode diameter of $40 \mu\text{m}$ and drizzle up to $\sim 150\text{-}\mu\text{m}$ diameter was being produced (Fig. 14b). Inside the line, some drizzle drops were still observed, but so were ice particles up to 2-mm diameter, along with a significant reduction in the number of $30\text{--}40\text{-}\mu\text{m}$ -diameter cloud droplets.

The fact that these observations indicated a supercooled liquid cloud devoid of ice with a cloud-top temperature of -15°C is especially noteworthy. Such conditions are expected to be highly susceptible to

glaciogenic cloud seeding. Interestingly in this case, the PPI scan from the DOW in Fig. 14a also revealed a line echo *parallel* to the flight track of the UWKA, between 20 and 50 km downwind of Packer John. This echo developed prior to the time seeding material had been transported that far downwind and was oriented perpendicular to the expected orientation of any possible seeding signature. It also developed directly along the location of the repeated flight track of the UWKA. We believe this line may be the result of aircraft-produced ice particles (APIPs; Rangno and Hobbs 1983, 1984; Woodley et al. 1991; Heymsfield et al. 2011) generated by the UWKA's propellers as it passed through the tops of the supercooled cloud.

A key component of SNOWIE is to evaluate and improve the AgI

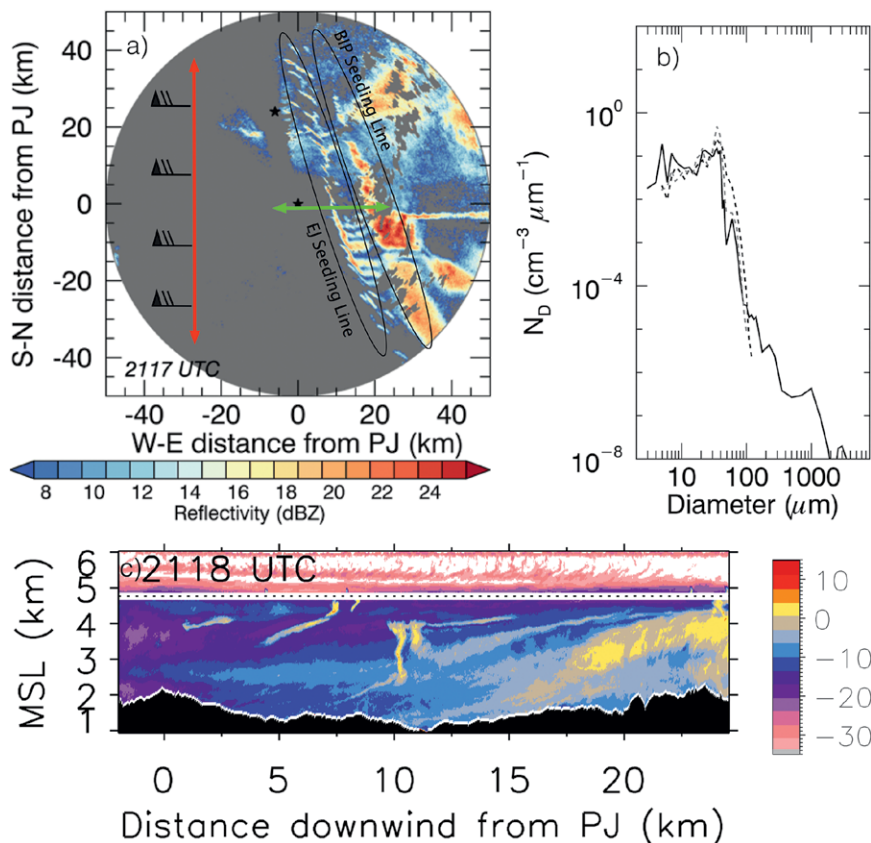


FIG. 14. As in Fig. 13, but for IOP 9, specifically at (a) 2117 UTC for the DOW PPI and (c) 2118 UTC for the WCR reflectivity. The seeding aircraft repeated its track twice: first from south to north and then from north to south. Note that at this time shown, the radar echo from the second seeding line is still elevated above the level of this PPI scan and therefore only shows echo from the first of the two tracks.

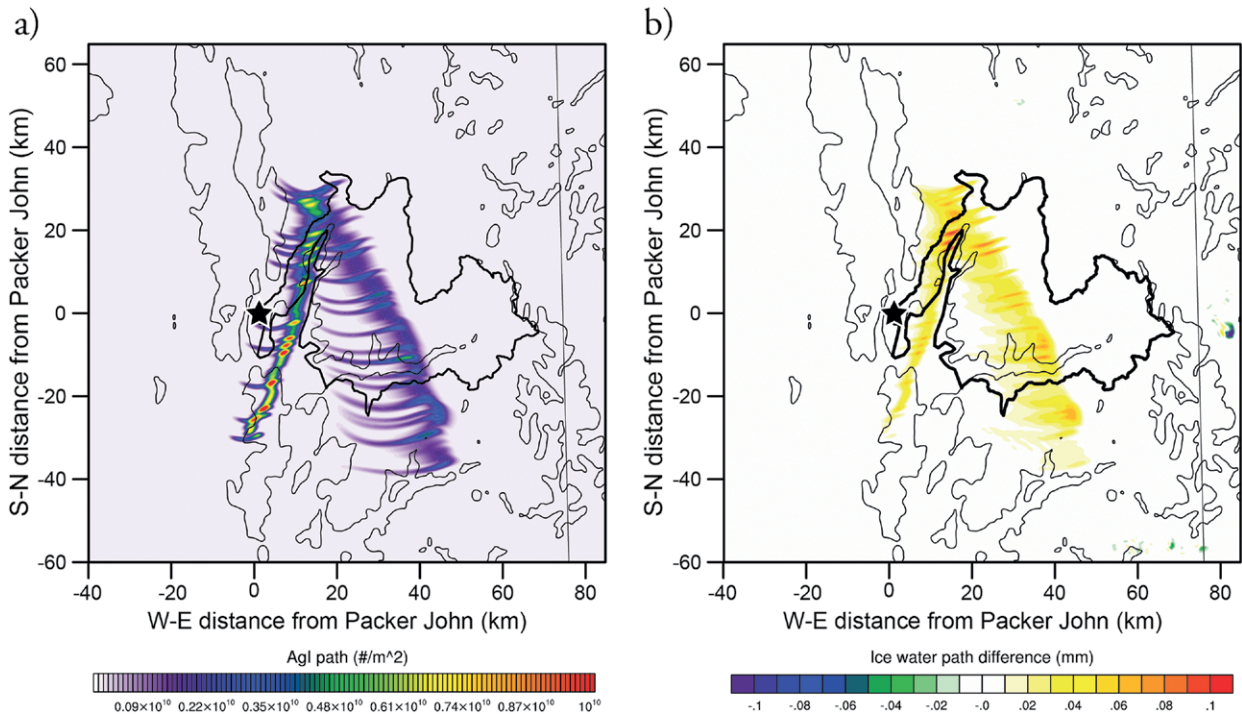


FIG. 15. Model simulation results from IOP 9 at 2120 UTC 31 Jan 2017 in the innermost domain (with 300-m grid spacing) showing (a) the vertically integrated dry AgI areal density (m^{-2}) and (b) the difference of vertically integrated ice-phase mass areal density (kg m^{-2}) between seeding and control simulations. The map domain is plotted in kilometers relative to Packer John, where Packer John DOW site is identified by a black star. Terrain height contours are thin black lines, starting at 1,000 m MSL and are every 500 m, and the Payette basin is overlaid as a thick black contour. Note that these maps show vertically integrated quantities, and therefore, both of the two AgI tracks are visible, as opposed to what is shown in the DOW PPI scan from the same time in Fig. 14. The AgI from the second track is more concentrated (as well as elevated) since it has not yet dispersed as much as that from the first track.

cloud-seeding parameterization in WRF so that it can be utilized to evaluate the impacts of cloud seeding. In the IOPs with clearly observed seeding signatures, such as those highlighted above, the model is currently being used to simulate the impacts of seeding, in very high resolution, to compare with the observations. An example of such simulations is shown for IOP 9 in Fig. 15. A description of the model configuration and setup for this numerical experiment is provided in Table 2. In this example, the model simulated the zigzag nature of the two tracks of the AgI plume, as well as the complicated and horizontally displaced dispersion of the AgI from BIP versus EJ flares due to the strong wind shear, similar to that observed by the DOW radar (Figs. 14 and 15). The model also simulated a cloud with supercooled liquid that, when and where AgI was introduced, was converted into ice and snow, also shown in the UWKA measurements (Fig. 15). The model's ability to accurately simulate the atmospheric conditions, such as the vertical and horizontal extent of the supercooled cloud, its liquid and ice water content, and the wind shear in this case,

will be critical to its ability to accurately simulate the response from seeding. Moreover, aspects of the cloud-seeding parameterization itself, such as the ice nucleation scheme, AgI activation scheme, and the scavenging and diffusion parameters, all play a role in how well the model can simulate AgI seeding impacts. These are areas in which we hope to make advances in scientific understanding by utilizing SNOWIE data to evaluate and improve the AgI cloud-seeding parameterization.

In cases where the seeding signatures are less apparent, we plan to use the model to guide where seeding impacts, if any, may be expected for closer inspection of the observations. Furthermore, beyond the areas where seeding impacts were observed, we also aim to evaluate the model's overall ability to accurately simulate cloud physical properties, such as hydrometeor phase, concentrations, and particle size distributions, as well as cloud dynamical properties, such as vertical velocity and turbulence, using the detailed measurements collected by the probes and WCR on the UWKA.

TABLE 2. Description of the model simulation configuration and setup.

| | 2,700-m domain | 900-m domain | 300-m domain |
|---------------------------------------|---|---|---|
| Model version | WRF, version 3.7.1 | WRF v3.7.1 | WRF v3.7.1 |
| Horizontal grids | 540 × 360 | 450 × 300 | 480 × 480 |
| Time step | 10 s | 3 s | 1/8 s |
| Driving data | ERA-Interim | One-way nest from 2.7-km domain WRF outputs | Nested within 900-m domain |
| Simulation time | 24 h from 0000 UTC 31 Jan to 0000 UTC 1 Feb 2017 | 11 h from 1200 UTC to 2300 UTC 31 Jan 2017 | 11 h from 1200 UTC to 2300 UTC 31 Jan 2017 |
| Vertical coordinate | 81 terrain-following eta levels | | |
| Land surface model | Noah MP | | |
| Radiation | RRTMG longwave and shortwave | | |
| Planetary boundary layer (PBL) scheme | MYNN | MYNN | — (LES) |
| Microphysics | Thompson–Eidhammer (TE; Thompson and Eidhammer 2014) with Cooper (1986) ice nucleation option | TE and TE with AgI seeding parameterization (Xue et al. 2013a,b) with Cooper (1986) ice nucleation option | TE and TE with AgI seeding parameterization (Xue et al. 2013a,b) with Cooper (1986) ice nucleation option |

SUMMARY. SNOWIE is a unique example of an integration of publicly funded and privately funded resources. This partnership resulted in the collection of a robust dataset available to both academic researchers and IPC that will provide the basis for innovative investigations on winter orographic cloud physics and the efficacy of cloud seeding. The partnership greatly enhanced both groups’ research opportunities without hindering the operational side of the IPC cloud-seeding program. Moreover, a substantial part of the project’s success is attributed to the strong collaboration with IPC staff, who contributed highly valuable local knowledge of the weather in the region toward forecasting for the project, as well as facilitated remarkable local area logistical support.

SNOWIE’s unique approach capitalized on recent advances in meteorological instrumentation and numerical modeling, such as the WCR and AgI cloud-seeding parameterization, with an innovative plan to collect in situ measurements of the impacts of cloud-seeding material released from a seeding aircraft in a manner that resulted in unambiguous seeding signatures in radar reflectivity. A major success in SNOWIE was that seeding signatures were observed in multiple IOPs, allowing the impacts of seeding to be investigated in many scenarios and providing support for the interpretation that signatures in the data were indeed impacts from the airborne seeding. Detailed analyses are currently under way to determine if signatures are detectable in additional IOPs where natural background radar reflectivity features are already present. Key components of the

experimental design that led to this success were 1) the location of the DOW radars atop an upwind ridge, which provided critical observations across the basin despite the complex terrain; 2) having one DOW dedicated to rapidly scanning RHIs parallel to the wind and along the UWKA flight track, which tracked fast-evolving processes; 3) flying the UWKA parallel to the wind with a vertically scanning cloud radar, allowing for in situ particle measurements and high-resolution radar depiction of the clouds; and 4) the use of airborne seeding, from which an unambiguous seeding pattern was dispersed.

The data and results from SNOWIE will be instrumental in addressing the long-standing questions regarding the effectiveness of winter orographic cloud seeding to augment precipitation. A comprehensive evaluation of the effectiveness of cloud seeding is a multistep process that starts with affirming the physical chain of events due to seeding and ends with determining how much additional precipitation (or subsequent streamflow) can be gained by seeding over a watershed. The results from SNOWIE to date have demonstrated the first step (French et al. 2018), and future work utilizing SNOWIE data and the cloud-seeding parameterization aims to continue chipping away at these critical questions to quantify the impacts of cloud seeding.

ACKNOWLEDGMENTS. We would like to acknowledge the many people and organizations that contributed tremendous and tireless efforts to make the field campaign a success, enabling data collection during cold and windy

snowstorms in remote mountainous areas: the DOW radar crew from the Center for Severe Weather Research (CSWR), in particular, Dr. Karen Kosiba, Dr. Joshua Wurman, Traeger Meyer, Marcus Guitierrez, Andrew Frambach, and Paul Robinson; the UWKA crew from the University of Wyoming, in particular, Dr. Sam Haimov, Dr. Larry Oolman, Dr. David Plummer, Matt Burkhart, Zane Little, Brent Glover, Ben Heesen, Tom Drew, and Brett Wadsworth; the staff and seeding aircraft crew from WMI, in particular, Bruce Boe, Jody Fischer, Brook Mueller, Jacob Mitchem, Brian Kindrat, Chance Faul, Brad Waller, Jeff Ceratto, Adam Brainard, Jack McPartland, and Dan Gilbert; the IPC forecasters and field crew, in particular, Nick Dawson, Brandal Glenn, Albert Pittman, Robert Walters, Matt Fletcher, Sean Elliott, and Howard Pennington; the NCAR field crew, Scott Landolt and Al Jachcik; and Frank McDonough from the Desert Research Institute (DRI). Additionally, undergraduate and graduate students from the University of Colorado Boulder, University of Illinois at Urbana-Champaign, University of Wyoming, and New Mexico Institute of Mining and Technology helped operate and deploy instruments during the field campaign.

Funding for CSWR DOWs and UWKA was provided through the National Science Foundation (NSF) Grants AGS-1361237 and AGS-1441831, respectively. IPC provided funding for the WMI seeding aircraft as well as several ground-based instruments (i.e., precipitation gauges, radiometers, rawinsondes, AgI ground generators, AINC, Boise State University snow sampling). The research was supported under NSF Grants AGS-1547101, AGS-1546963, and AGS-1546939 and by the IPC. The Federal Aviation Administration (FAA) provided funding for two radiometers and the supercooled liquid water sondes. This research is in response to requirements and funding by the FAA. The views expressed are those of the authors and do not necessarily represent the official policy or position of the FAA.

REFERENCES

- Aikins, J., K. Friedrich, B. Geerts, and B. Pokharel, 2016: Role of a cross-barrier jet and turbulence on winter orographic snowfall. *Mon. Wea. Rev.*, **144**, 3277–3300, <https://doi.org/10.1175/MWR-D-16-0025.1>.
- Boe, B., J. A. Heimbach Jr., T. W. Krauss, L. Xue, X. Chu, and J. T. McPartland, 2014: The dispersion of silver iodide particles from ground-based generators over complex terrain. Part I: Observations with acoustic ice nucleus counters. *J. Appl. Meteor. Climatol.*, **53**, 1325–1341, <https://doi.org/10.1175/JAMC-D-13-0240.1>.
- Borys, R. D., D. H. Lowenthal, and D. L. Mitchell, 2000: The relationships among cloud microphysics, chemistry, and precipitation rate in cold mountain clouds. *Atmos. Environ.*, **34**, 2593–2602, [https://doi.org/10.1016/S1352-2310\(99\)00492-6](https://doi.org/10.1016/S1352-2310(99)00492-6).
- Breed, D., R. Rasmussen, C. Weeks, B. Boe, and T. Deshler, 2014: Evaluating winter orographic cloud seeding: Design of the Wyoming Weather Modification Pilot Project (WWMPP). *J. Appl. Meteor. Climatol.*, **53**, 282–299, <https://doi.org/10.1175/JAMC-D-13-0128.1>.
- Chu, X., B. Geerts, L. Xue, and R. Rasmussen, 2014: Radar observations and WRF LES simulations of the impact of ground-based glaciogenic seeding effect on orographic clouds and precipitation: Part I: Observations and model validations. *J. Appl. Meteor. Climatol.*, **53**, 2264–2286, <https://doi.org/10.1175/JAMC-D-14-0017.1>.
- , —, —, and B. Pokharel, 2017a: A case study of cloud radar observations and large-eddy simulations of a shallow stratiform orographic cloud, and the impact of glaciogenic seeding. *J. Appl. Meteor. Climatol.*, **56**, 1285–1304, <https://doi.org/10.1175/JAMC-D-16-0364.1>.
- , —, —, and R. Rasmussen, 2017b: Large-eddy simulations of the impact of ground-based glaciogenic seeding on shallow orographic convection: A case study. *J. Appl. Meteor. Climatol.*, **56**, 69–84, <https://doi.org/10.1175/JAMC-D-16-0191.1>.
- Chubb, T. H., S. T. Siems, and M. J. Manton, 2011: On the decline of wintertime precipitation in the snowy mountains of southeastern Australia. *J. Hydrometeorol.*, **12**, 1483–1497, <https://doi.org/10.1175/JHM-D-10-05021.1>.
- Cooper, W. A., 1986: Ice initiation in natural clouds. *Precipitation Enhancement—A Scientific Challenge*, Meteor. Monogr., No. 43, Amer. Meteor. Soc., 29–32.
- Dennis, A. S., 1980: *Weather Modification by Cloud Seeding*. International Geophysics Series, Vol. 24, Academic Press, 267 pp.
- Deshler, T., and D. W. Reynolds, 1990: The persistence of seeding effects in a winter orographic cloud seeded with silver iodide burned in acetone. *J. Appl. Meteor.*, **29**, 477–488, [https://doi.org/10.1175/1520-0450\(1990\)029<0477:TPOSEI>2.0.CO;2](https://doi.org/10.1175/1520-0450(1990)029<0477:TPOSEI>2.0.CO;2).
- , —, and A. W. Huggins, 1990: Physical response of winter orographic clouds over the Sierra Nevada to airborne seeding using dry ice or silver iodide. *J. Appl. Meteor.*, **29**, 288–330, [https://doi.org/10.1175/1520-0450\(1990\)029<0288:PROWOC>2.0.CO;2](https://doi.org/10.1175/1520-0450(1990)029<0288:PROWOC>2.0.CO;2).
- Fisher, J. M., M. L. Lytle, M. L. Kunkel, D. R. Blestrud, N. W. Dawson, S. K. Parkinson, R. Edwards, and S. G. Benner, 2018: Assessment of ground-based and aerial cloud seeding using trace chemistry. *Adv. Meteor.*, **2018**, 7293987, <https://doi.org/10.1155/2018/7293987>.

- French, J. R., and Coauthors, 2018: Precipitation formation from orographic cloud seeding. *Proc. Natl. Acad. Sci. USA*, **115**, 1168–1173, <https://doi.org/10.1073/pnas.1716995115>.
- Friedrich, J., E. A. Kalina, J. Aikins, J. Sun, D. Gochis, P. Kucera, K. Ikeda, and M. Steiner, 2016: Raindrop size distribution and rain characteristics during the 2013 Great Colorado Flood. *J. Hydrometeorol.*, **17**, 53–72, <https://doi.org/10.1175/JHM-D-14-0184.1>.
- Garstang, M., and Coauthors, 2003: *Critical Issues in Weather Modification Research*. National Academies Press, 123 pp.
- , R. Bruintjes, R. Serafin, H. Orville, B. Boe, W. Cotton, and J. Warburton, 2005: Weather modification: Finding common ground. *Bull. Amer. Meteor. Soc.*, **86**, 647–655, <https://doi.org/10.1175/BAMS-86-5-647>.
- Geerts, B., and Coauthors, 2013: The AgI Seeding Cloud Impact Investigation (ASCII) campaign 2012: Overview and preliminary results. *J. Wea. Modif.*, **45**, 24–43.
- Grant, L. O., and R. E. Elliott, 1974: The cloud seeding temperature window. *J. Appl. Meteor.*, **13**, 355–363, [https://doi.org/10.1175/1520-0450\(1974\)013<0355:TCSTW>2.0.CO;2](https://doi.org/10.1175/1520-0450(1974)013<0355:TCSTW>2.0.CO;2).
- Heysmsfield, A. J., G. Thompson, H. Morrison, A. R. Bansemmer, R. M. Rasmussen, P. Minnis, Z. Wang, and D. Zhang, 2011: Formation and spread of aircraft-induced holes in clouds. *Science*, **333**, 77–81, <https://doi.org/10.1126/science.1202851>.
- Hobbs, P. V., J. H. Lyons, J. D. Locatelli, K. R. Biswas, L. F. Radke, R. R. Weiss Sr., and A. L. Rangno, 1981: Radar detection of cloud-seeding effects. *Science*, **213**, 1250–1252, <https://doi.org/10.1126/science.213.4513.1250>.
- Holmes, J., 2012: Urban Sustainability Initiative Rep., 12 pp., <http://digitalscholarship.unlv.edu/reports/6>.
- Ikeda, K., R. M. Rasmussen, W. D. Hall, and G. Thompson, 2007: Observations of freezing drizzle in extratropical cyclonic storms during IMPROVE-2. *J. Atmos. Sci.*, **64**, 3016–3043, <https://doi.org/10.1175/JAS3999.1>.
- Jing, X., and B. Geerts, 2015: Dual-polarization radar data analysis of the impact of ground-based glaciogenic seeding on winter orographic clouds. Part II: Convective clouds. *J. Appl. Meteor. Climatol.*, **54**, 2034–2056, <https://doi.org/10.1175/JAMC-D-15-0056.1>.
- , —, K. Friedrich, and B. Pokharel, 2015: Dual-polarization radar data analysis of the impact of ground-based glaciogenic seeding on winter orographic clouds. Part I: Mostly stratiform clouds. *J. Appl. Meteor. Climatol.*, **54**, 1944–1969, <https://doi.org/10.1175/JAMC-D-14-0257.1>.
- , —, and B. Boe, 2016: The extra-area effect of orographic cloud seeding: Observational evidence of precipitation enhancement downwind of the target mountain. *J. Appl. Meteor. Climatol.*, **55**, 1409–1424, <https://doi.org/10.1175/JAMC-D-15-0188.1>.
- Keeler, J. M., B. F. Jewett, R. M. Rauber, G. M. McFarquhar, R. M. Rasmussen, L. Xue, C. Liu, and G. Thompson, 2016a: Dynamics of cloud-top generating cells in winter cyclones. Part I: Idealized simulations in the context of field observations. *J. Atmos. Sci.*, **73**, 1507–1527, <https://doi.org/10.1175/JAS-D-15-0126.1>.
- , —, —, —, —, —, —, and —, 2016b: Dynamics of cloud-top generating cells in winter cyclones. Part II: Radiative and instability forcing. *J. Atmos. Sci.*, **73**, 1529–1553, <https://doi.org/10.1175/JAS-D-15-0127.1>.
- , —, —, —, —, —, —, and —, 2017: Dynamics of cloud-top generating cells in winter cyclones. Part III: Shear and convective organization. *J. Atmos. Sci.*, **74**, 2879–2897, <https://doi.org/10.1175/JAS-D-16-0314.1>.
- Kenny, J. F., N. L. Barber, S. S. Hutson, K. S. Linsey, J. K. Lovelace, and M. A. Maupin, 2009: Estimated use of water in the United States in 2005. U.S. Geological Survey Circular 1344, 52 pp.
- Kerr, R. A., 1982: Cloud seeding: One success in 35 years. *Science*, **217**, 519–521, <https://doi.org/10.1126/science.217.4559.519>.
- Langer, G., 1973: Evaluation of NCAR ice nucleus counter. Part I: Basic operation. *J. Appl. Meteor.*, **12**, 1000–1011, [https://doi.org/10.1175/1520-0450\(1973\)012<1000:EONINC>2.0.CO;2](https://doi.org/10.1175/1520-0450(1973)012<1000:EONINC>2.0.CO;2).
- Liu, C., and Coauthors, 2016: Continental-scale convection-permitting modeling of the current and future climate of North America. *Climate Dyn.*, **49**, 71–95, <https://doi.org/10.1007/s00382-016-3327-9>.
- Löffler-Mang, M., and J. Joss, 2000: An optical disdrometer for measuring size and velocity of hydrometeors. *J. Atmos. Oceanic Technol.*, **17**, 130–139, [https://doi.org/10.1175/1520-0426\(2000\)017<0130:AODFMS>2.0.CO;2](https://doi.org/10.1175/1520-0426(2000)017<0130:AODFMS>2.0.CO;2).
- , M. Kunz, and W. Schmid, 1999: On the performance of a low-cost K-band Doppler radar for quantitative rain measurements. *J. Atmos. Oceanic Technol.*, **16**, 379–387, [https://doi.org/10.1175/1520-0426\(1999\)016<0379:OTPOAL>2.0.CO;2](https://doi.org/10.1175/1520-0426(1999)016<0379:OTPOAL>2.0.CO;2).
- Pokharel, B., and B. Geerts, 2016: A multi-sensor study of the impact of ground-based glaciogenic seeding on clouds and precipitation over mountains in Wyoming. Part I: Project description. *Atmos. Res.*, **182**, 269–281, <https://doi.org/10.1016/j.atmosres.2016.08.008>.

- , —, and X. Jing, 2014a: The impact of ground-based glaciogenic seeding on orographic clouds and precipitation: A multisensor case study. *J. Appl. Meteor. Climatol.*, **53**, 890–909, <https://doi.org/10.1175/JAMC-D-13-0290.1>.
- , —, —, K. Friedrich, J. Aikins, D. Breed, R. Rasmussen, and A. Huggins, 2014b: The impact of ground-based glaciogenic seeding on clouds and precipitation over mountains: A multi-sensor case study of shallow precipitating orographic cumuli. *Atmos. Res.*, **147–148**, 162–182, <https://doi.org/10.1016/j.atmosres.2014.05.014>.
- , —, —, —, K. Ikeda, and R. Rasmussen, 2017: A multi-sensor study of the impact of ground-based glaciogenic seeding on clouds and precipitation over mountains in Wyoming. Part II: Seeding impact analysis. *Atmos. Res.*, **183**, 42–57, <https://doi.org/10.1016/j.atmosres.2016.08.018>.
- Politovich, M. K., and G. Vali, 1983: Observations of liquid water in orographic clouds over Elk Mountain. *J. Atmos. Sci.*, **40**, 1300–1312, [https://doi.org/10.1175/1520-0469\(1983\)040<1300:OOLWIO>2.0.CO;2](https://doi.org/10.1175/1520-0469(1983)040<1300:OOLWIO>2.0.CO;2).
- Ralph, F. M., and Coauthors, 2017: Atmospheric rivers emerge as a global science and applications focus. *Bull. Amer. Meteor. Soc.*, **98**, 1969–1973, <https://doi.org/10.1175/BAMS-D-16-0262.1>.
- Rangno, A. L., and P. V. Hobbs, 1983: Production of ice particles in clouds due to aircraft penetrations. *J. Climate Appl. Meteor.*, **22**, 214–232, [https://doi.org/10.1175/1520-0450\(1983\)022<0214:POIPIC>2.0.CO;2](https://doi.org/10.1175/1520-0450(1983)022<0214:POIPIC>2.0.CO;2).
- , and —, 1984: Further observations of the production of ice particles in clouds by aircraft. *J. Climate Appl. Meteor.*, **23**, 985–987, [https://doi.org/10.1175/1520-0450\(1984\)023<0985:FOOTPO>2.0.CO;2](https://doi.org/10.1175/1520-0450(1984)023<0985:FOOTPO>2.0.CO;2).
- Rasmussen, R. M., and Coauthors, 2011: High-resolution coupled climate runoff simulations of seasonal snowfall over Colorado: A process study of current and warmer climate. *J. Climate*, **24**, 3015–3048, <https://doi.org/10.1175/2010JCLI3985.1>.
- , and Coauthors, 2018: Evaluation of the Wyoming Weather Modification Pilot Project (WWMPP) using two approaches: Traditional statistics and ensemble modeling. *J. Appl. Meteor. Climatol.*, **57**, 2639–2660, <https://doi.org/10.1175/JAMC-D-17-0335.1>.
- Rauber, R. M., 1992: Microphysical structure and evolution of a central Sierra Nevada orographic cloud system. *J. Appl. Meteor.*, **31**, 3–24, [https://doi.org/10.1175/1520-0450\(1992\)031<0003:MSAEOA>2.0.CO;2](https://doi.org/10.1175/1520-0450(1992)031<0003:MSAEOA>2.0.CO;2).
- , and L. O. Grant, 1987: Supercooled liquid water structure of a shallow orographic cloud system in southern Utah. *J. Climate Appl. Meteor.*, **26**, 208–215, [https://doi.org/10.1175/1520-0450\(1987\)026<0208:SLWSOA>2.0.CO;2](https://doi.org/10.1175/1520-0450(1987)026<0208:SLWSOA>2.0.CO;2).
- Reynolds, D. W., 2015: Literature review and scientific synthesis on the efficacy of winter orographic cloud seeding. U.S. Bureau of Reclamation Tech. Memo., 148 pp., www.usbr.gov/main/qoi/docs/Literature_Review_and_Scientific_Synthesis_of_the_Efficacy_of_Winter_Orographic_Cloud_Seeding_Peer_Review.pdf.
- Rosenfeld, D., and Coauthors, 2013: The common occurrence of highly supercooled drizzle and rain near the coastal regions of the western United States. *J. Geophys. Res. Atmos.*, **118**, 9819–9833, <https://doi.org/10.1002/jgrd.50529>.
- Schaefer, V. J., 1946: The production of ice crystals in a cloud of supercooled water droplets. *Science*, **104**, 457–459, <https://doi.org/10.1126/science.104.2707.457>.
- Serke, D., and Coauthors, 2014: Supercooled liquid water content profiling case studies with a new vibrating wire sonde compared to a ground-based microwave radiometer. *Atmos. Res.*, **149**, 77–87, <https://doi.org/10.1016/j.atmosres.2014.05.026>.
- Solheim, F., J. R. Godwin, E. R. Westwater, Y. Han, S. J. Keihm, K. Marsh, and R. Ware, 1998: Radiometric profiling of temperature, water vapor and cloud liquid water using various inversion methods. *Radio Sci.*, **33**, 393–404, <https://doi.org/10.1029/97RS03656>.
- Steenburgh, W. J., and T. R. Blazek, 2001: Topographic distortion of a cold front over the Snake River Plain and central Idaho mountains. *Wea. Forecasting*, **16**, 301–314, [https://doi.org/10.1175/1520-0434\(2001\)016<0301:TDOACF>2.0.CO;2](https://doi.org/10.1175/1520-0434(2001)016<0301:TDOACF>2.0.CO;2).
- Strapp, J. W., W. R. Leaitch, and P. S. K. Liu, 1992: Hydrated and dried aerosol-size-distribution measurements from the Particle Measuring Systems FSSP-300 probe and the deiced PCASP-100X probe. *J. Atmos. Oceanic Technol.*, **9**, 548–555, [https://doi.org/10.1175/1520-0426\(1992\)009<0548:HADASD>2.0.CO;2](https://doi.org/10.1175/1520-0426(1992)009<0548:HADASD>2.0.CO;2).
- Super, A. B., and B. A. Boe, 1988: Microphysical effects of wintertime cloud seeding with silver iodide over the Rocky Mountains. Part III: Observations over the Grand Mesa, Colorado. *J. Appl. Meteor.*, **27**, 1166–1182, [https://doi.org/10.1175/1520-0450\(1988\)027<1166:MEOWCS>2.0.CO;2](https://doi.org/10.1175/1520-0450(1988)027<1166:MEOWCS>2.0.CO;2).
- , and A. W. Huggins, 1992: Investigations of the targeting of ground-released silver iodide in Utah—Part I: Ground observations of silver-in-snow and ice nuclei. *J. Wea. Modif.*, **24**, 19–34.
- Tessendorf, S. A., B. Boe, B. Geerts, M. J. Manton, S. Parkinson, and R. Rasmussen, 2015: The future

- of winter orographic cloud seeding: A view from scientists and stakeholders. *Bull. Amer. Meteor. Soc.*, **96**, 2195–2198, <https://doi.org/10.1175/BAMS-D-15-00146.1>.
- Thompson, G., and T. Eidhammer, 2014: A study of aerosol impacts on clouds and precipitation development in a large winter cyclone. *J. Atmos. Sci.*, **71**, 3636–3658, <https://doi.org/10.1175/JAS-D-13-0305.1>.
- Vonnegut, B., 1947: The nucleation of ice formation by silver iodide. *J. Appl. Phys.*, **18**, 593–595, <https://doi.org/10.1063/1.1697813>.
- Wang, Z., and Coauthors, 2012: Single aircraft integration of remote sensing and in situ sampling for the study of cloud microphysics and dynamics. *Bull. Amer. Meteor. Soc.*, **93**, 653–668, <https://doi.org/10.1175/BAMS-D-11-00044.1>.
- Ware, R., R. Carpenter, J. Guldner, J. Liljegren, T. Nehrkorn, F. Solheim, and F. Vandenberghe, 2003: A multichannel radiometric profiler of temperature, humidity, and cloud liquid. *Radio Sci.*, **38**, 8079, <https://doi.org/10.1029/2002RS002856>.
- Woodley, W. L., T. J. Henderson, B. Vonnegut, G. Gordon, R. E. Breidenthal, and S. H. Holle, 1991: Aircraft-produced ice particles (APIPs) in supercooled clouds and the probable mechanism for their production. *J. Appl. Meteor.*, **30**, 1469–1489, [https://doi.org/10.1175/1520-0450\(1991\)030<1469:APIPS>2.0.CO;2](https://doi.org/10.1175/1520-0450(1991)030<1469:APIPS>2.0.CO;2).
- Xue, L., and Coauthors, 2013a: Implementation of a silver iodide cloud seeding parameterization in WRF: Part I: Model description and idealized 2D sensitivity tests. *J. Appl. Meteor. Climatol.*, **52**, 1433–1457, <https://doi.org/10.1175/JAMC-D-12-0148.1>.
- , and Coauthors, 2013b: Implementation of a silver iodide cloud seeding parameterization in WRF: Part II: 3D simulations of actual seeding events and sensitivity tests. *J. Appl. Meteor. Climatol.*, **52**, 1458–1476, <https://doi.org/10.1175/JAMC-D-12-0149.1>.
- , and Coauthors, 2017: WRF large-eddy simulations of chemical tracer deposition and seeding effect over complex terrain from ground- and aircraft-based AgI generators. *Atmos. Res.*, **190**, 89–103, <https://doi.org/10.1016/j.atmosres.2017.02.013>.
- Zhu, Y., and R. E. Newell, 1998: A proposed algorithm for moisture fluxes from atmospheric rivers. *Mon. Wea. Rev.*, **126**, 725–735, [https://doi.org/10.1175/1520-0493\(1998\)126<0725:APAFMF>2.0.CO;2](https://doi.org/10.1175/1520-0493(1998)126<0725:APAFMF>2.0.CO;2).

“It has become clear that natural disasters are at the very center of the problem of economic and social development.”

— TYLER COWEN, *Professor of Economics, George Mason University*

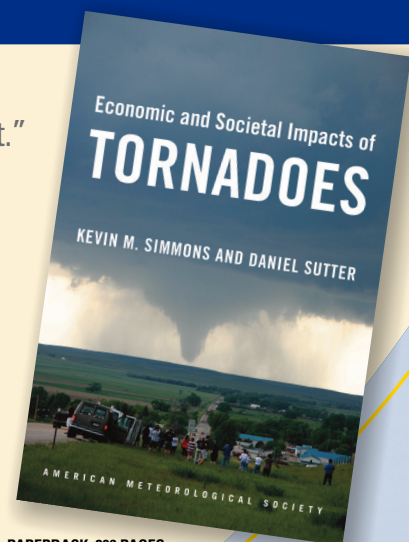
Economic and Societal Impacts of Tornadoes

KEVIN M. SIMMONS AND DANIEL SUTTER

Approximately 1,200 tornadoes touch down across the United States annually, and for almost a decade, economists Simmons and Sutter have been gathering data from sources such as NOAA and the U.S. Census to examine their economic impacts and social consequences. Their unique database has enabled this fascinating and game-changing study for meteorologists, social scientists, emergency managers, and everyone studying severe weather, policy, disaster management, or applied economics.

Featuring:

- Social science perspective of tornado impacts
- Evaluation of NWS warnings and efforts to reduce casualties
- Statistical analysis of effectiveness of warning lead time, shelters, and more



© 2011, PAPERBACK, 296 PAGES
 ISBN: 978-1-878220-99-8
 AMS CODE: ESIT
 LIST \$30 MEMBER \$22

AMS BOOKS

RESEARCH APPLICATIONS HISTORY

www.ametsoc.org/amsbookstore